HAL open science

Adenylates regulate Arabidopsis plastidial thioredoxin activities through the binding of a CBS domain protein.

Kevin Baudry, Félix Barbut, Séverine Domenichini, Damien Guillaumot, Mai Pham Thy, Hélène Vanacker, Wojciech Majeran, Anja Krieger-Liszkay, Emmanuelle Issakidis-Bourguet, Claire Lurin

To cite this version:

Kevin Baudry, Félix Barbut, Séverine Domenichini, Damien Guillaumot, Mai Pham Thy, et al.. Adenylates regulate Arabidopsis plastidial thioredoxin activities through the binding of a CBS domain protein.. Plant Physiology, 2022, 189 (4), pp.2298-2314. 10.1093/plphys/kiac199 . hal-03866164

HAL Id: hal-03866164

https://hal.science/hal-03866164v1

Submitted on 22 Nov 2022

HAL is a multi-disciplinary open access archive for the deposit and dissemination of scientific research documents, whether they are published or not. The documents may come from teaching and research institutions in France or abroad, or from public or private research centers.

L'archive ouverte pluridisciplinaire **HAL**, est destinée au dépôt et à la diffusion de documents scientifiques de niveau recherche, publiés ou non, émanant des établissements d'enseignement et de recherche français ou étrangers, des laboratoires publics ou privés.

Short title: CBSX2 regulates Thioredoxins m in plastids

Title:

Adenylates regulate Arabidopsis plastidial thioredoxin activities through the binding of a CBS domain protein

Author names and affiliations:

Kevin Baudry[a,b], Félix Barbut[a,b], Séverine Domenichini[a,b,c], Damien Guillaumot[a,b], Mai Pham Thy[a,b], Hélène Vanacker[a,b], Wojciech Majeran[a,b], Anja Krieger-Liszkay[d], Emmanuelle Issakidis-Bourguet[a,b,*], Claire Lurin[a,b]

[a]Université Paris-Saclay, CNRS, INRAE, Univ Evry, Institute of Plant Sciences Paris-Saclay (IPS2), 91190, Gif sur Yvette, France.

[b]Université Paris Cité, CNRS, INRAE, Institute of Plant Sciences Paris-Saclay (IPS2), 91190, Gif sur Yvette, France.

[c]Present address: Université Paris-Saclay, UMS IPSIT - US 31 INSERM - UMS 3679 CNRS

[d] Université Paris-Saclay, Institute for Integrative Biology of the Cell (I2BC), CEA, CNRS, 91198 Gif-sur-Yvette, France

***Corresponding author:**

Emmanuelle Issakidis-Bourguet, IPS2, rue de Noetzlin, CS 80004, 91192 Gif sur Yvette Cedex, tel: +33 1 69 15 33 37, email: emmanuelle.issakidis-bourguet@universite-paris-saclay.fr

Author contributions: C. L., E. I-B., W. M., H. V. and A. K-L. designed the research and supervised the experiments; F. B., S. D., D. G. and M. P. T. performed experiments;. K. B., A. K-L. and E. I-B performed experiments and analyzed the data; K. B., C. L., A. K-L. and E. I-B. wrote the manuscript.

Fundings: K.B. research was supported by a French Ph. D. fellowship from "Ministère de la Recherche et de l'Enseignement Supérieur". D.G. research was supported by a post-doctoral fellowship from a French State grant (Saclay Plant Sciences, reference n° ANR-17-EUR-0007, EUR SPS-GSR) managed by the French National Research Agency under an Investments for the Future program (reference n° ANR-11-IDEX-0003-02). The IPS2 and the I2BC benefit from the support of the Labex Saclay Plant Sciences-SPS (ANR-17-EUR-0007). This work was supported by the French Infrastructure for Integrated Structural Biology (FRISBI; grant number ANR-10-INSB-05).

33 **One-sentence summary:** A cystathionine-β-synthase protein inhibits thioredoxins m
34 activities towards NADP-malate dehydrogenase and 2-Cys peroxiredoxin in an adenylate-
35 dependent manner.
36 .

ABSTRACT

Cystathionine-β-synthase (CBS) domains are found in proteins of all living organisms and were proposed to play a role as energy sensors regulating protein activities through their adenosyl ligand binding capacity. In plants, members of the CBSX protein family carry a stand-alone pair of CBS domains. In Arabidopsis, CBSX1 and CBSX2 are targeted to plastids where they were proposed to regulate thioredoxins (TRX). TRX are ubiquitous cysteine thiol oxido-reductases involved in the redox-based regulation of numerous enzymatic activities as well as in the regeneration of thiol-dependent peroxidases. In Arabidopsis, 10 TRX isoforms were identified in plastids and divided in five sub-types.

Here, we show that CBSX2 specifically inhibits the activities of m-type TRXs towards two chloroplast TRX-related targets. By testing activation of NADP-malate dehydrogenase and reduction of 2-Cys peroxiredoxin, we found that TRX m1/2 inhibition by CBSX2 was alleviated in presence of AMP or ATP.

We also evidenced, by pull-down assays, a direct interaction of CBSX2 with reduced TRX m1 and m2 that was abolished in presence of adenosyl ligands. In addition, we report that, in comparison to wild-type plants, the Arabidopsis T-DNA double mutant *cbsx1 cbsx2* exhibits growth and chlorophyll accumulation defects in cold conditions, suggesting a function of plastidial CBSX proteins in plant stress adaptation. Altogether, our results show an energy sensing regulation of plastid TRX m activities by CBSX, possibly allowing a feedback regulation of ATP homeostasis via activation of cyclic electron flow in the chloroplast, to maintain a high energy level for an optimal growth.

INTRODUCTION

Plants depend on light for the generation of energy and reducing power in the forms of ATP and NADPH produced in the chloroplasts and consumed in assimilatory processes.

The major role played by chloroplasts as the source and target of reduction–oxidation (redox) regulation is now well established in plant cells (Baier and Dietz, 2005). Thioredoxins (TRX) are key actors of the underlying complex redox regulatory network. TRX are small (~12kDa) ubiquitous redox proteins found in all cellular compartments. Among the 20 isoforms encoded by the Arabidopsis (*Arabidopsis thaliana*) genome, 10 are targeted to plastids and were sub-divided in five groups (4 TRX m, 2 TRX f, 2 TRX y, 1 TRX x and 1 TRX z). In plastids, TRX have numerous targets involved in various metabolic and stress response functions (Gelhaye et al., 2005; Lemaire et al., 2007; Geigenberger et al., 2017). TRX can act either as regulators of the activity of their targets by post-translational modification or as reducing substrate for their target. TRX can activate their targets through direct disulfide bridge reduction, as for example, plastidial NADPH-dependent malate dehydrogenase (NADP-MDH). They can also provide reducing power to their targets as in case of the 2-cysteine peroxiredoxin (2-Cys PRX) (Collin et al., 2003; Collin et al., 2004).

While the number of functions attributed to TRX in plastids is very large (Montrichard et al., 2009), knowledge about their regulation is limited. In plastids, TRXs redox state mainly depends on the balance between the "electron pressure" light-fueled by the photosynthetic electron transport chain and the "oxidative pressure" of H_2O_2 (Vaseghi et al., 2018; Yoshida and Hisabori, 2018). Data about additional factors directly regulating TRX redox state are very scarce. For instance, TRX f was found glutathionylated and consequently losing its capability to regulate its targets (Michelet et al., 2005). Yoo *et al.* (2011) suggested that the CBSX proteins are ubiquitous regulators of TRXs in plastids to control H_2O_2 levels and regulate lignin polymerization in the anther endothecium.

Cystathionine-β-synthase (CBS) domain (Pfam: PF00571) was identified in proteins from bacteria, yeasts, animals and plants (Ignoul and Eggermont, 2005; Kushwaha et al., 2009; Crozet et al., 2014; Shahbaaz et al., 2015). This small domain of approximately 60 amino acids forms an antiparallel β-sheet flanked by helices on one side. It is generally found as a tandem repeat forming a CBS pair or the so-called Bateman domain (Bateman, 1997) that defines the CBS-Domain-Containing-Protein (CDCP) family (Ignoul and Eggermont, 2005). Homodimers of CBS pairs are generally involved in the binding of regulatory adenosyl ligands such as AMP, ATP or S-adenosylmethionine (Kemp, 2004; Ereño-Orbea et al., 2013).

Consequently, CBS domains were proposed to function as sensors of cell energy status (Scott et al., 2004; Kushwaha et al., 2009). Associated to several different functional domains, in a wide range of functionally different CDCP proteins, CBS domains act generally as regulatory domains of protein activity through adenosyl ligand binding (Hardie and Hawley, 2001; Scott et al., 2004; Ignoul and Eggermont, 2005; Buey et al., 2017). For examples, the highly conserved eukaryotic energy sensor AMPK/SNF1/SnRK1 is regulated by its γ-subunit composed of four CBS domains in tandem (Polge and Thomas, 2007; Ramon et al., 2013; Crozet et al., 2014). In mammals, AMP/ADP binding to the CBS domains of the AMP-activated protein kinase (AMPK) induces a conformational change that stabilizes the phosphorylated activation loop of the protein by upstream kinases (Hardie and Hawley, 2001; Ignoul and Eggermont, 2005; Xiao et al., 2011).

The Arabidopsis genome encodes 34 CDCPs each containing one or two pairs of CBS domains that are generally closely associated with other functional protein domain(s). In these proteins, CBS domains are expected to regulate the molecular function of other adjacent domains. In contrast, the members of the CBSX subfamily of CDCP proteins carry a stand-alone pair of CBS domains and are thus supposed to perform their regulatory function through protein interactions (Kushwaha et al., 2009). In Arabidopsis, the six members of the CBSX subfamily were proposed to be localized in several cellular compartments. Indeed, whereas CBSX1 and CBSX2 were shown to be plastid targeted (Yoo et al., 2011; Jung et al., 2013), CBSX3 was recently shown to be localized in mitochondria (Shin et al., 2020), CBSX4 is predicted to be cytosolic and CBSX5 and CBSX6 are expected to be located in the endoplasmic reticulum (Ok et al., 2012).

The two Arabidopsis plastidial CBSX, CBSX1 (AT4G36910) and CBSX2 (AT4G34120), share 91% similarity and 74% identity in their amino acid sequences. Crystal structures of Arabidopsis CBSX1 and CBSX2 were solved and showed that these two proteins form anti-parallel (*head-to-tail*) homodimers exhibiting similar quaternary structures (Jeong et al., 2013a; Jeong et al., 2013b).

To characterize CBSX1 and CBSX2 functions, Yoo *et al.* (2011) identified candidate protein interactors using yeast 2-hybrid. Among them, were several chloroplast thioredoxins (TRX) for which interactions were confirmed by *in vitro* pull-down assays and *in planta* bimolecular fluorescence complementation (BiFC) experiments (Yoo et al., 2011; Jung et al., 2013). Both CBSX1 and CBSX2 were shown to increase the activity of TRX m2, TRX f1, TRX x and TRX y1 in a standard TRX activity assay based on bovine insulin reduction. These activities were enhanced in presence of AMP (Yoo et al., 2011). Similarly, it was shown that CBSX3

enhances the *in vitro* activity of the mitochondrial TRX o1 and TRX o2 (Yoo et al., 2011; Shin et al., 2020). Physiological functions of plastidial CBSX proteins were investigated in transformed Arabidopsis over-expressing *CBSX1* and *CBSX2*. These plants exhibited a sterile phenotype related to anther indehiscence. A defect in endotecium secondary cell wall thickening during anther development was observed in over-expressors and linked to insufficient reactive oxygen species (ROS) accumulation (Yoo et al., 2011; Jung et al., 2013). *CBSX3* knockdown lines surprisingly presented a similar sterile phenotype related to an anther indehiscence defect (Yoo et al., 2011; Jung et al., 2013; Shin et al., 2020). Plant sterility of CBSX1 and CBSX2 overexpressors, on one hand, and CBSX3 knockdown, on the other hand, is supposedly linked to improper thioredoxin activities in plastids or in mitochondria (Yoo et al., 2011; Jung et al., 2013; Shin et al., 2020).

Despite the previous in depth molecular characterization of the plastidial CBSX structures and the demonstration of their interaction with TRX, the functional and physiological relevance of CBSX regulatory role on TRX activities remains questioned. In this study, by evaluating plastid CBSX regulation of TRX-dependent activities *in vitro* using two physiologically-relevant targets of plastidial TRX, we show that CBSX2 specifically inhibits TRX m activities and that this effect is reversed by ATP and, to a lesser extent, by AMP. Adenylates impairing direct CBSX-TRX interaction, we propose a model in which CBSX2 specifically inhibits reduced TRX m to maintain chloroplast energy status (ATP) for optimal plant growth during acclimation to low temperature.

RESULTS

Phylogenetic Analysis of AtCBSX

To investigate relationships between the 6 Arabidopsis CBSX proteins, we constructed a maximum likelihood phylogenetic tree from their full-length amino acid sequences. Our analysis suggests that CBSX proteins that are localized in the same subcellular compartment are closer in the phylogenetic tree than CBSX targeted to different locations (Figure S1). In particular, the two closest Arabidopsis CBSX proteins, CBSX1 and CBSX2, share 74% of amino acid sequence identity (similarity 91%). They were both shown to be targeted to the chloroplasts (Yoo et al., 2011; Jung et al., 2013). The closest protein of the plastidial CBSX group, CBSX3, shares 26% of amino acid sequence identity with CBSX2 (similarity 44%) and is localized in mitochondria. CBSX4, (also known as AtPV42b) is a close homolog of AtPV42a, a γ-type subunit of SnRK1 containing two CBS pairs (Fang et al., 2011). Accordingly, it appears to be a non canonical CBSX standing apart in our phylogenetic tree. This tree focused on the Arabidopsis CBSX subfamily is consistent with the wide phylogenetic analysis made on the 34 CDCPs of *A. thaliana* and the 59 CDCPs of *Oryza sativa* (Kushwaha et al., 2009).

CBSX1 and CBSX2 are able to form homomers and heteromers in plastids

We first confirmed the subcellular location of the chloroplast and mitochondrial CBSX isoforms. Transiently transformed *Nicotiana benthamiana* leaves with CBSX-RFP fusions were observed by confocal microscopy. Consistently with previous studies and predictions (Yoo et al., 2011; Jung et al., 2013), fluorescence signals of full-length CBSX1-RFP and CBSX2-RFP co-localized with the chlorophyll fluorescence of chloroplasts (Figure S2). In contrast, the CBSX3-RFP fluorescence signal was observed as spots outside the chloroplasts consistently with the recent finding from Shin *et al.* (2020) showing a mitochondrial localization of CBSX3 (Figure S2).

Crystal structures of CBSX1 and CBSX2 previously showed that these two proteins form homodimers with highly similar structures. The high similarity of their amino-acid sequences suggests that they may also form heterodimers. We investigated this possibility in a yeast 2-hydrid (Y2H) assay. CBSX1, CBSX2 and CBSX3 lacking their predicted organelle target peptides were fused to Gal4 activation and DNA binding domains and expressed in relevant Y2H strains. In a mating-based Y2H matricial assay, we showed that CBSX1 and CBSX2 can form homomers as well as heteromers (Figure 1). In contrast, we did not identify any interaction involving CBSX3, neither homomeric nor heteromeric.

To confirm these interactions in plant cells, we performed bimolecular fluorescence complementation (BiFC) analysis. *Nicotiana benthamiana* leaves were transiently co-transformed with full-length CBSX1 and CBSX2 fused at their C-termini to either the N-ter moiety (nYFP) or the C-ter moiety (cYFP) of the yellow fluorescent protein. To enhance YFP signals, plants were also co-transformed with HC-Pro, an inhibitor of gene silencing (Stephan et al., 2011). Four days after transformation, specific chloroplastic YFP signals were observed in both homomeric combinations (Figure 2). To test heteromerisation of CBSX1 and CBSX2, two YFP combinations were tested. YFP signals were only observed when CBSX2-nYFP and CBSX1-cYFP fusion proteins were co-expressed. The reciprocal combination did not give any signal. Consistently with CBSX localization, signals were observed in plastids. For each interaction signal, a spectral analysis of at least two spots was performed to confirm the YFP fluorescence signature.

Altogether our results confirm that both CBSX1 and CBSX2 are targeted to plastid where they form homomers as well as heteromers.

CBSX2 inhibits the ability of TRX m to activate NADP-MDH and AMP modulates this effect

CBSX1 and CBSX2 proteins were previously found to activate TRX-dependent insulin reduction (Yoo et al., 2011). Here, we investigated the ability of CBSX proteins to modulate physiologically-relevant plastid TRX-dependent enzyme activities. To this aim, we produced and purified recombinant his-tagged CBSX1 and CBSX2 in a bacterial expression system. Untagged TRXs and TRX-regulated NADP-MDH were also obtained as previously described (Collin et al., 2003). All proteins were produced without their target peptide. NADP-MDH was previously shown to be efficiently activated *in vitro* by the members of the TRX m and TRX f subfamilies (Collin et al., 2003) and its regulation by TRX f1, TRX m1 and TRX m2 was validated *in planta* (Thormählen et al., 2015; Thormählen et al., 2017). The plastid TRX-regulated MDH uses NADPH as a cofactor to reduce oxaloacetate (OAA) into malate. Its activation is strictly TRX dependent and requires the reduction of two constitutive regulatory disulfide bonds, and a third transient disulfide (Issakidis et al., 1994; Ruelland et al., 1997). Here, we tested the ability of five TRX isoforms (TRX m1, TRX m2, TRX m4, TRX f1 and TRX f2) to activate MDH in presence or absence of CBSX. We incubated MDH with DTE-reduced TRX, with or without addition of CBSX for 20 min prior to measuring MDH activity. We checked that activation kinetics were linear and did not reach a plateau within 20 min of incubation (Figure S3). We defined the MDH activation rate as the value of the initial activity

212 slope calculated after activation treatment. Our results show that CBSX1 does not have any
213 significant effect on the capacity of the five TRXs tested to activate NADP-MDH (Figure 3A-
214 E). In contrast, CBSX2 inhibits the enzyme activation by TRX m1 or TRX m2 or TRX m4
215 (Figure 3A-C), but not by TRX f1 or TRX f2 (Figure 3D,E). In presence of CBSX2 with TRX
216 m1, TRX m2 or TRX m4, NADP-MDH activation was reduced to 30-60% of the maximum
217 activation reached in absence of CBSX2 (Figure 3A-C). Because CBS domains were shown
218 to bind several adenosyl ligands (Ignoul and Eggermont, 2005) and, specifically, CBSX2
219 structure was shown to be strongly modified upon AMP binding (Jeong et al., 2013a), we
220 tested the effect of this adenylate on the TRX limitation exerted by CBSX2. While TRX-
221 dependent MDH activation was not significantly affected by AMP (Figures 3 and S4), we
222 found that AMP limited the inhibitory effect of CBSX2 on TRX m (Figure 3A-C). Indeed,
223 TRX m-dependent MDH activation could reach 65-80% of its maximum in presence of
224 CBSX2 and AMP at a concentration of 1 mM, a concentration commonly used
225 experimentally to test regulation of CDCPs by adenylate ligands (Yoo et al., 2011; Jung et al.,
226 2013; Buey et al., 2017).

227 **CBSX2 directly regulates TRX activities**

228 Our results showed that CBSX2 selectively inhibits TRXs m but not TRXs f in their
229 capacities to activate NADP-MDH. They strongly suggested an inhibitory action of CBSX2
230 on TRX instead of a direct inhibition of MDH activity. To confirm these results, we took
231 advantage of a mutant form of NADP-MDH, the DMC (Double Mutation C-terminus)-MDH,
232 in which the two cysteines that form the C-terminal regulatory disulfide bond are substituted
233 by serines. The DMC-MDH has a basal enzyme activity without any activating treatment, but
234 reduced TRX is required to reach full activity (Issakidis et al., 1994). Without treatment, or in
235 presence of DTE alone, DMC-MDH exhibits *ca.* 25% of the activity reached after a 20 min
236 activation treatment in presence of TRX m1 (Figure 4). When DMC-MDH was incubated
237 with CBSX2 and DTE, its activity remained unchanged (Figure 4) confirming that CBSX2
238 does not directly inhibit DMC-MDH activity. We also checked that AMP had no direct effect
239 on DMC-MDH activity (Figure S5). By contrast, DMC-MDH activation by TRX m1 or TRX
240 m2, like for the wild-type enzyme, was strongly impaired in presence of CBSX2, and AMP
241 limited this effect (Figure 4). Taken together our results strongly support a specific role
242 played by CBSX2 as a negative regulator of TRXs m, with AMP acting as a modulator.

243 **Adenosyl nucleotides differentially modulate TRX m inhibition by CBSX2**

244 Noticeably, we found that AMP alleviates the CBSX2 effect on TRXs m only partially in our
245 experimental conditions. The AMP concentration (1 mM) commonly used in this kind of
246 experiments corresponds to a concentration by far higher than reported AMP concentrations
247 in the chloroplast that do not exceed 1 µM (Stitt et al., 1982). Thus, we also tested AMP at
248 lower concentrations, as well as other adenylate nucleotides, *e.g.* ADP and ATP prevailing in
249 the chloroplast (Figure 5). At 1 mM, we found that all adenylates could suppress the
250 inhibitory effect of CBSX2 (Figure 5), while they had no significant effect on TRX m1-
251 dependent activation of NADP-MDH (without CBSX) (Figure S4). At 1 mM, a physiological
252 concentration for ATP in the chloroplast, ATP could totally inhibit the effect of CBSX2
253 (Figure S6). We also tested MgATP, since *in vivo* 95-99 % of ATP is predicted to be
254 complexed with Mg^{2+}, and we also found its strong effect on TRX m. Interestingly, by testing
255 lower concentrations of adenylate nucleotides, we could evidence that they have differential
256 effects on CBSX2 (Figure 5). Indeed, at 10 µM, ATP, but neither AMP nor ADP, had an
257 effect, and at 50 µM, AMP and ATP, but not ADP, restricted CBSX2 inhibition. At 1 mM,
258 ATP was significantly more efficient than ADP to limit CBSX2 inhibition. Thus, our data
259 suggest that AMP may not exert any effect on CBSX2 at physiologically relevant
260 concentrations. They also suggested that ADP may be much less efficient than ATP in
261 limiting CBSX2 effect on TRX, estimated concentrations of ADP and ATP in the chloroplast
262 ranging from 0.5 to 0.8 mM and 0.8 to 1.2 mM, respectively (Stitt et al., 1982; Voon et al.,
263 2018). We also tested the effect of ATP together with ADP on the time course of NADP-
264 MDH activation in presence of CBSX2, at adenylate concentrations and ratios corresponding
265 to light and dark conditions prevailing in the chloroplast (Usuda, 1988) (Figure S7). Again,
266 CBSX2 effect was attenuated in presence of adenylates and, clearly, the effect was more
267 pronounced in the light mimicking condition compared to the dark mimicking condition.

268 **CBSX2 inhibits TRX m-dependent reductive regeneration of 2-Cys PRX**

269 TRXs can regulate the activity of their targets (like NADP-MDH) and they can also provide
270 electrons to thiol-dependent peroxidases named peroxiredoxins (PRX). It was previously
271 shown that plastidial TRXs can reduce 2-Cys PRX *in vitro* with various efficiencies (Collin et
272 al., 2003; Collin et al., 2004; Bohrer et al., 2012). To extend CBSX function towards TRXs ,
273 we also tested other TRX isoforms that do not regulate NADP-MDH, *e.g.* TRX y1 and TRX
274 x, for their capacity to serve as reducing substrate for 2-Cys PRX (obtained as described in
275 Collin et al., 2003) in presence of CBSX. We found that PRX activities measured without

276 TRX (DTT alone) in absence and in presence of CBSX were very similar, showing that
277 neither CBSX1 nor CBSX2 has any direct effect on 2-Cys PRX reduction of tBOOH (an
278 alkyl-hydroperoxide) (Figure 6A). When combining PRX, TRX and CBSX proteins, we
279 found that the addition of CBSX1 had no effect on the peroxidase activity, and that TRX f1,
280 TRX y1 or TRX x were not affected by CBSX2 (Figure 6B-D). Similarly to its effect when
281 testing NADP-MDH activation, CBSX2 inhibited TRX m1-dependent reduction of the 2-Cys
282 PRX (Figure 6E). We also tested NTRC, a physiological substrate for this target, and found
283 that it was not significantly affected by CBSX2 (Figure 6F). As for NADP-MDH activation,
284 the addition of AMP restricted the inhibitory effect of CBSX2 on TRX m1 (Figure 7). These
285 results show that CBSX2 is able to specifically inhibit TRX m in serving as reducing
286 substrate for 2-Cys PRX and that, like in NADP-MDH activation, an adenylate nucleotide can
287 prevent this effect.

288 **Direct interaction between CBSX2 and TRX m1 proteins is modulated by adenosyl**
289 **ligands**

290 It was previously reported that CBSXs directly interact with TRXs (Yoo et al., 2011; Jung et
291 al., 2013; Shin et al., 2020). To validate these interactions and further investigate the effect of
292 adenosyl ligands, we performed pull-down assays with 6His-CBSXs and TRXm1 in presence
293 or absence of AMP or ATP. After incubation of TRX m1 and CBSX2 in reducing conditions
294 (presence of DTE), proteins were mixed with nickel affinity resin. After washings, they co-
295 eluted from the resin (Figure 8A). In contrast, interaction between CBSX2 and TRX m1 was
296 not observed when the incubation was performed in absence of a chemical reductant. Notably,
297 interaction was also abolished in presence of 1 mM AMP or ATP (Figure 8A,B). Similar
298 experiments were performed using 6His-CBSX1 and TRX m1, and no interaction was
299 detected (Figure 8B). Taken together these results show that CBSX2, but not CBSX1, is able
300 to interact with reduced TRX m1 in absence of ATP or AMP. These observations are
301 consistent with the specific inhibitory effect of CBSX2 on TRX m1 activities (NADP-MDH
302 activation and 2-Cys PRX reduction) and suggest that adenyl ligands can modulate TRX m
303 inhibition by CBSX2 by preventing CBSX-TRX direct interaction. Notably, the absence of
304 effect of CBSX1 on TRXs could be linked to the lack of interaction between these two
305 proteins.

The double mutant *cbsx1 cbsx2* is smaller and exhibits chlorophyll accumulation defects at low temperature

To investigate the role of CBSX in connection with TRX related functions *in planta*, we characterized *cbsx1* and *cbsx2* Arabidopsis T-DNA insertion mutants. These mutants were previously described in Yoo *et al.* (2011) and Jung *et al.* (2013), respectively, and did not show any macroscopic phenotype at the rosette stage. Because we suspected functional redundancy between the two CBSX plastid isoforms and found that they can form heteromers *in vivo* (Figure 2), we crossed the corresponding single mutants to obtain the *cbsx1 cbsx2* double mutant. In standard long day growth conditions, single and double mutants showed no obvious phenotypes compared to wild-type (WT) plants (Figure 9A), as previously reported under short day or continuous light (Yoo et al 2011; Jung et al 2013; Murai et al. 2021). Because *CBSX1* and *CBSX2* genes were reported to exhibit an increased level of expression at low temperature (ePlant database; (Waese et al., 2017)), the double mutant was germinated and grown at 12°C. In this condition, the *cbsx1 cbsx2* double mutant rosettes were slightly smaller and pale green in comparison with the WT (Col-0 ecotype) or single mutant plants (Figure 9B). These differences were confirmed by comparing rosette fresh-weights and chlorophyll contents of the double mutant, which were significantly decreased compared to single mutants and WT plants (Figure 9C,D). These results suggest that both CBSX1 and CBSX2 are required for normal growth and chloroplast functions at low temperature.

The double mutant *cbsx1 cbsx2* shows altered P700 oxidation and reduction kinetics

Since TRXs m were proposed as specific regulators of the photosynthetic electron transport, we investigated whether it was altered in *cbsx1 cbsx2*. We followed oxidation and re-reduction of P700, the primary electron donor of photosystem I, by absorption spectroscopy in the near infrared, in this double mutant, compared to WT and to TRX mutants (double mutant *trxm1 trxm2* and single mutant *trxm4*). As shown in figure 10A, upon onset of actinic light, the first fast transient oxidation level of P700 was higher in *cbsx1 cbsx2* than in WT and *trxm1 trxm2*. Then a drop of the signal below the baseline, showing ferredoxin reduction, was observed in all genotypes. This drop was followed by a multiphasic increase of the signal until a steady state level of $P700^+$ was reached. It is striking that in *cbsx1 cbsx2* this steady state level was reached much faster than in the other genotypes. Illumination with far-red light, exciting preferentially photosystem I, led to the same oxidation level in all genotypes, with *trxm1 trxm2* reaching the maximum level of $P700^+$ slower than WT and *cbsx1 cbsx2*. Then far-red light was turned off and a saturating flash was given to achieve the same maximum P700 oxidation level in all genotypes. We observed clear differences in the

oxidation kinetics between genotypes, showing that the pool of electron donors to photosystem I available in *cbsx1 cbsx2* is smaller than in WT and *trxm1 trxm2*. This may be interpreted as a sign of lower cyclic electron flow in *cbsx1 cbsx2*.

Next, we measured the rates of $P700^+$ re-reduction after illumination of dark-adapted leaves with far-red light. The re-reduction of $P700^+$ after 1 min far-red illumination was much slower in *cbsx1 cbsx2* than in WT, while in TRX mutants *trxm1 trxm2* and *trxm4* it was faster than in WT as previously found in the same mutant lines Thormählen et al., 2017; Courteille et al., 2013) (Figure 10B and S9). This indicates a lower reduction state of the plastoquinone pool after far-red illumination in *cbsx1 cbsx2* and can be interpreted as a lower cyclic flow in *cbsx1 cbsx2* compared with the other genotypes.

Taken together, both the P700 oxidation in actinic light and its re-reduction after far-red light indicate that the electron transport chain is more oxidized in *cbsx1 cbsx2* and that in *cbsx1 cbsx2* lower cyclic flow takes place, both under actinic and far-red illumination.

354 **DISCUSSION**

355 Arabidopsis CBSX proteins were previously shown as regulatory interactors of chloroplastic
356 TRXs. However, their function was characterized using a non-physiological reduction assay.
357 Here, in order to understand the physiological function of CBSX1 and CBSX2 towards TRXs,
358 we tested the chloroplast TRX targets NADP-MDH and 2-Cys PRX. We show that CBSX2
359 specifically inhibits the activity of m-type TRXs, but does not have any effect on other
360 plastidial TRX isoforms (TRX f, TRX x and TRX y) and NTRC. In the same experimental
361 conditions, CBSX1 had no effect on tested TRX activities suggesting a different function for
362 this CBSX isoform in the chloroplast. Interestingly, despite its high sequence and structure
363 similarity with CBSX2, CBSX1 was shown to present some differences especially in the
364 relative angle between the monomers (Jeong et al., 2013b) that may be responsible for distinct
365 functionalities between the two isoforms. However, we cannot totally exclude that our
366 CBSX1 protein preparation, although obtained following exactly the same methodology as for
367 CBSX2, could be inactive.

368

369 We found that both ADP and ATP are able to alleviate CBSX2 inhibition of TRX m, at
370 physiologically relevant concentrations, with a stronger effect of ATP. In chloroplasts, ATP is
371 produced by the thylakoid membrane ATP synthase complex from ADP and inorganic
372 phosphate. Upon illumination, a rapid increase in the level of ATP accompanied by a marked
373 decrease in AMP and a slight decrease in ADP were observed (Santarius and Heber, 1965;
374 Kobayashi et al., 1979; Voon et al., 2018). This raise in ATP levels in chloroplasts in the light
375 and the higher efficiency of ATP in modulating CBSX effect on TRX suggest that ATP is the
376 major ligand of CBSX2 in plant cells. Generally, CDCPs, like AMPKγ, that bind AMP or
377 ATP are affected by both but exhibit differential affinity (Scott et al., 2004). Although crystal
378 structure analysis suggested that CBSX2 cannot bind ATP (Jeong et al., 2013a), our data
379 clearly show a modulating effect of ATP onto CBSX2 functions towards TRXs m. ATP
380 probably binds to CBSX2 and ATP-bound CBSX2 crystal structure might validate this
381 possibility in the future.

382 We found a relationship between protein-protein as well as ligand-protein interactions and
383 functional inhibitory effects, allowing us to propose a model integrating molecular
384 interactions in the mechanism of TRX m inhibition by CBSX2 (Figure 11). When ATP
385 concentration is low, CBSX2 is able to interact with reduced TRX m. This interaction inhibits
386 TRX m ability to reduce its targets. Since CBSX proteins are devoid of any Cys residue the
387 hypothesis of a competition between CBSX2 and targets for electron transfer from TRX can

be ruled out. Instead, a competition between CBSX2 and a TRX target may occur at the surface of TRX, or interaction of CBSX2 with TRX m may induce a conformational change of the TRX that would be unfavorable for electron transfer and/or target interaction. The CBSX2 structure in complex with AMP, solved at 2.2Å resolution, appeared to be approximately flat, with a strong reshaping of the protein upon AMP binding (Jeong et al., 2013a). This could be also hypothesized for ATP binding. Thus, when ligand concentration is high, CBSX2 protein would undergo a conformational change that may prevent interaction with TRX. Our model based on direct protein-protein interaction would explain the specificity of the inhibition of TRX m by CBSX2.

In planta, by measuring leaf NADP-MDH activity (extractable and maximal) and 2-Cys PRX redox state (monomer/dimer status and over-oxidation), we found no clear difference in *cbsx* mutant leaves compared to wild-type plants cultivated at control or at low temperature (Figure S8). This result suggests that in our growth conditions these two targets might be principally regulated by TRX isoforms other than TRXs m, or NTRC, as already reported *in vitro* and *in vivo* (Collin et al., 2003; Pulido et al., 2010; Yoshida et al., 2015; Pérez-Ruiz et al., 2017). Recent genetic studies have allowed investigating specifically the roles of TRXs m *in vivo* and point to their role in regulating the proton motive force (pmf). pmf primarily drives ATP synthesis and is a prerequisite for light-dependent activation of ATP synthase (CF1-γ reduction) by TRXs m and f (Junesch and Gräber, 1987; Sekiguchi et al., 2020). TRX m1 and m2 would be necessary for full activation of photosynthesis during the high light periods where elevated levels of reduced photosystem I (PSI) acceptors favor cyclic electron transport (CET) (Thormählen et al., 2017). By recycling electrons from ferredoxin to the thylakoid plastoquinone (PQ) pool via PQ reductases, PSI-CET allows maintaining the appropriate pH range of the thylakoid lumen contributing to the ΔpH causal to the pmf that drives ATP synthase. Since ATP synthesis occurs without production of NADPH, PSI-CET is important to maintain an optimal ATP/NADPH ratio to meet metabolic demand and thereby optimal plant growth (Yamori and Shikanai, 2016). Notably, when the *trxm1_m2_m4* triple mutant was compared to the wild-type, Okegawa and Motohashi (2015) found that the ATP level was higher in the light, and the initial rate of light-dependent CF1-γ reduction was slowed down (Sekiguchi et al., 2020). Data obtained in Arabidopsis show that both PQ reductase pathways, namely the Proton Gradient Regulation 5 (PGR5)/PGRL1 complex and the NADH dehydrogenase-like complex (NDH), contribute to supply sufficient acceptors from PSI (Shikanai, 2016). While a predominant role is played by the PGR5/PGRL1 pathway in normal

growth conditions (Nakano et al., 2019), NDH is believed to protect the photosynthetic apparatus at chilling stress under low irradiance when ΔpH is low (Yamori et al., 2011; Yamori et al., 2015). Courteille *et al.* (2013) reported that Tobacco TRX m overexpressing plants are characterized by a down regulation of PSI-CET via the NDH pathway while NDH-dependent PQ reduction was up-regulated in Arabidopsis mutant plants specifically lacking TRX m4. It was proposed that TRXs m may promote reduction of dimeric PGRL1 to its monomeric activated form (Hertle et al., 2013) and interaction of TRX m1 with PGRL1 has been shown *in planta* (Nikkanen et al., 2018). Recently, Okegawa and Motohashi, confirmed the regulation of the PGR5/PGRL1 complex by m-type TRXs and reported that TRX m4 downregulates the PGR5/ PGRL1-dependent pathway via a direct interaction with PGRL1 (2020). Here, we found that, compared to wild-type, TRX m lacking plants (*trxm1m2* double mutant and *trxm4* single mutant) exhibited a faster $P700^+$ reduction (Figure 10B and Figure S9), similarly to previously reported data (Courteille et al., 2013). On the contrary, the *cbsx1 cbsx2* mutant showed a slower reduction indicative of decreased oxidation of the PQ pool favorable for PSI-CET. Thus, CBSX affects P700 photo-oxidation reduction cycle in PSI. By avoiding accumulation of electrons in the PQ pool, CBSX would allow maintaining a pH range in the luminal space of the thylakoid membrane appropriate for ATP synthesis (Miyake, 2020).

At low temperature, transcriptomics databases indicate a higher expression level of *CBSX1* and *CBSX2* genes (Waese et al., 2017) while transcripts abundance for TRX m1, TRX m2 and TRX m4 are decreased (Dreyer and Dietz, 2018). When we investigated the *cbsx1 cbsx2* mutants growth at low temperature (12°C), and under a weak illumination (60 µmol photons.m^{-2}.s^{-1}) to avoid photoinhibition, we found that the double mutant exhibited growth and chlorophyll accumulation defects in these conditions. These phenotypes may be caused by a suppression of PSI-CET. Noticeably, PSI-CET is enhanced in pea leaves by chilling (Cornic et al., 2000), as in rice, where NDH-dependent cyclic electron flow plays a significant role for photosynthesis and plant growth at low temperature (Yamori et al., 2011). Moreover, both pathways of PSI-CET protect tomato leaves against photoinhibition when exposed to chilling stress (Wang et al., 2020).

Notably, impaired growth and decreased chlorophyll content were found in tobacco over-expressing TRX m (Rey et al., 2013). Da *et al.* (2017) reported a high pmf in TRX m-deficient Arabidopsis plants and Thormälen *et al.* (2017) found that in *trx m1m2* mutants PSI yield was enhanced and accompanied by an increased oxidation of the PQ pool, indicative of PSI-CET stimulation. Thus, in our chilling growth conditions (low temperature and low light

intensity), we believe that no damage of photosynthetic membranes occurred (no photoinhibition) and that a high PSI-CET was necessary to sustain ATP homeostasis and plant growth. Based on previous studies on TRXs m, this would imply alleviation of their negative regulation exerted on PSI-CET, and, based on the present work, we hypothesize that this would implicate CBSX proteins.

Interestingly, a recent work reported the role played by adenylates to balance the "plastid energy budget", supporting the view that PSI-CET is activated under conditions where stromal ATP is low, but is downregulated as ATP levels build up, allowing for effective ATP homeostasis (Fisher et al., 2019). Accordingly, we propose a model (Figure 12) in which CBSX2, acting as a sensor of the chloroplast energy status, would specifically decrease reduced TRX m activity when ATP concentration is low. This would consequently decrease TRX m-dependent negative regulation of PSI-CET to allow a higher pmf-driven ATP production, since TRXs f are not affected by CBSX2 and efficiently activate ATP synthase.

Overall, present findings reveal a new ATP sensing mechanism involving Cystathionine-β-synthase containing domain protein and thioredoxin possibly acting for optimal ATP homeostasis in the chloroplast.

MATERIALS AND METHODS

Plants Materials

T-DNA insertion mutants *cbsx1* (Gabi_050D12), *cbsx2* (Salk_136934), *trxm1 trxm2* (Salk_087118_ and Salk_123570), *trxm4* (Salk_0 532538) were previously described in Yoo *et al.* (2011), Jung *et al.* (2013), Thormählen *et al.* (2017), and Courteille *et al.* (2013), respectively. They were obtained from the NASC (Nottingham Arabidopsis Stock Centre) (Scholl et al., 2000). Plants are sown and grown under long days conditions (16h light/day) at 20°C or 12°C constant temperature. Light intensity was 60 µmol photons.m^{-2}.s^{-1} (tubular fluorescent lamps: Sylvania Lynx-LE 840, white light) at the level of the leaves.

Phylogenetic Analysis

We used TAIR10 models to determine the full-length amino acid sequences of the six *A. thaliana* CBSX: CBSX1 (AT4G36910), CBSX2 (AT4G34120), CBSX3 (AT5G10860), CBSX4 (AT1G80090), CBSX5 (AT4G27460) and CBSX6 (AT1G65320). The phylogenetic tree was inferred using the Maximum Likelihood method based on the Jones-Taylor-Thornton

488 (JTT) matrix-based model (Jones et al., 1992), bootstraps: 1000. Analysis were conducted on
489 MEGA7 (Kumar et al., 2016).

490 **Yeast 2-Hybrid**

491 *CBSX1* (72-236), *CBSX2* (72-238) and *CBSX3* (16-206) truncated ORF were amplified and
492 cloned into the pDONR207 vector using Gateway BP Clonase enzyme (Invitrogen). Primers
493 (ORF_intern + ORF_stop) were designed to amplify ORF encoding mature proteins lacking
494 their putative target peptide (prediction by TargetP 1.1 (Nielsen et al., 1997; Emanuelsson et
495 al., 2000). *CBSX* ORF were then subcloned into pDEST-AD-CYH2 and pDEST-DB
496 destination vectors (Dreze et al., 2010) using Gateway LR Clonase enzyme (Invitrogen)
497 according to manufacturer's instructions. Y8800 MATa and Y8930 MATα yeast strains
498 (James et al., 1996) were transformed with AD-ORF and DB-ORF, respectively. Yeast
499 mating and selection were performed according to the InterATOME platform pipeline as
500 previously described in Monachello *et al.* (2019). As positive interacting protein control we
501 used DB-mNUWA and AD-mDYW2 (Guillaumot et al., 2017).

502 **Bimolecular Fluorescence Complementation and Subcellular localization**

503 *CBSX1* (1-236), *CBSX2* (1-238) and *CBSX3* (1-206) full length ORF were amplified and
504 cloned into the pDONR207 vector using Gateway BP Clonase enzyme (Invitrogen). Primers
505 (ORF_start + ORF_end) were designed to amplify ORF without stop codon allowing C-
506 terminal fusion after Gateway LR transfert into pGreen-0229-RFP, pBiFC1 or pBiFC4
507 destination vectors (Boussardon et al., 2012). For subcellular localization, C58C1 pSOUP
508 *Agrobacterium tumefaciens* cells were transformed with pGreen-0229-RFP vectors. For
509 Bimolecular Fluorescence Complementation, C58C1 pMP90 *Agrobacterium tumefaciens*
510 cells were transformed with pBiFC1 and pBIFC4 vectors. For all experiments leaves of
511 *Nicotiana benthamiana* were co-infiltrated with agrobacteria containing required vectors and
512 the silencing inhibitor HC-Pro (Stephan et al., 2011). Leaves were observed 4 days after
513 transformation using a confocal microscope (Zeiss LSM 880). Image acquisition and image
514 analysis were performed using the IPS2 Imaging Facility.

515 **Protein Production and Purification**

516 *CBSX1* (72-236) and *CBSX2* (72-238) ORF in pDONR207 were subcloned into the
517 expression vector pDEST17 (Invitrogen) using Gateway LR Clonase enzyme (Invitrogen)
518 according to manufacturer's instructions. Protein production in *Escherichia coli* BL21 cells
519 was induced overnight at 30°C in LB medium containing 100 µg/mL carbenicilline and 400

520 µM IPTG. Bacteria lysis was performed in 30 mM Tris pH7.9 containing protease inhibitor
521 (complete Mini EDTA-free Roche®) using a French press. Proteins were purified by affinity
522 chromatography using a nickel column (GE healthcare® His-trap HP 1mL). Column washing
523 was performed with 30 mM Tris pH 7.9 containing 20 mM imidazole. Proteins elution was
524 performed with 30 mM Tris pH 7.9 containing 200 mM imidazole. Eluted proteins were
525 dialysed and concentrated in 30 mM Tris pH 7.9 using Amicon columns (Sigma Amicon
526 ultra-4 Z740191-8EA 30K). All TRX and 2-Cys PRX proteins were produced as previously
527 described in Collin *et al.* (2003; 2004). NTRC was obtained as described in Bohrer *et al.*,
528 2012. Fully activated wild-type MDH and mutant DMC-MDH recombinant enzymes,
529 obtained as previously described in Issakidis *et al.* (1994), had a specific activity (u/mg) of
530 368 +/- 42 and 386 +/- 25, respectively. 2-Cys PRX exhibited a K_{cat} of 179 +/- 17 s^{-1} with
531 TRXx as reducing substrate. All these values being very close to those previously reported
532 (Issakidis et al., 1994; Collin et al.,2003) certified that appropriate purified protein
533 preparations were used for the present study.

534 **MDH activity**

535 MDH (0.24 g/L) was activated by incubation with 10 mM DTE-reduced TRX with the
536 eventual addition of 30 µM CBSX and 1 mM AMP or ATP, as indicated, in 30 mM Tris
537 pH7.9 at 21°C. TRX concentration was 10 µM for all TRX excepted TRX f1 used at 1 µM. 3
538 µL aliquots of reaction medium were periodically withdrawn and added to 200 µL of 30°C
539 pre-heated reaction medium (for wild-type MDH: 160 µM NADPH, 750 µM OAA, 30 mM
540 Tris pH7.9 ; for DMC-MDH: 160 µM NADPH, 1 mM OAA, 30 mM Tris pH7.9).
541 Experiments with MgATP were performed by incubation with 1 mM ATP and 10 mM
542 $MgCl_2$. The MDH activity was measured by following the NADPH consumption at 340 nm
543 during 1 min in a Tecan infinite m200 PRO plate reader. Each experiment has been repeated
544 at least twice, with three to four technical replicates in each experiment. MDH activities
545 (initial velocities) were estimated as the slopes calculated during 20 seconds. When the
546 coefficient of variation of the estimated slope was higher than 15%, we discarded the data.
547 We defined TRX activity as the MDH activity after 20 minutes of activation. Statistical
548 analysis of MDH activity dataset was performed with a linear model taking into account TRX,
549 CBSX and adenylate effects.

550 **PRX activity**

551 0,4 mM of tBOOH (tert-butyl hydroperoxide) was reduced by 15 µM 2-Cys PRX A, 15 µM
552 of 0,5 mM DTE-reduced TRX, 45 µM CBSX and 1 mM AMP in 100 mM Tris pH7.9.

553 Unreduced tBOOH in 10 µL aliquots was periodically quantified at 560 nm using the FOX
554 coloration procedure described in Collin *et al.* (2004). CBSX direct effect on PRX was
555 assayed in presence of 1 mM DTE.

556 **Analysis of chlorophyll content**

557 Chlorophylls) quantification was performed by acetone extraction on 50 mg fresh rosette leaf
558 as previously described in Sumanta et al. (2014).

559 **P700 absorption**

560 The redox state of P_{700} was monitored by following differences of the 875 nm and 830 nm
561 transmittance signals using a DUAL-PAM-100 (Walz, Effeltrich, Germany). When P700
562 oxidation was measured with actinic light, plants were kept prior to the measurements in the
563 light in the growth chamber so that the Calvin-Benson cycle enzymes were active. When the
564 pool of electron donors was measured by following $P700^+$ re-reduction after far-red
565 illumination, plants were kept in the dark prior to the measurement to insure inactive Calvin-
566 Benson cycle enzymes. The acquisition rate was set to 1 ms.

567 **Statistical analysis**

568 All statistical analyses were conducted on R (version 3.2.5). To analyze each dataset, we used
569 ANOVA with several factors and when necessary statistical interactions were considered. To
570 control the family-wise error rate, p-values were adjusted using the Bonferroni procedure. A
571 difference was considered significant when its adjusted p-value was lower than 0.05.
572 For the MDH activities dataset with the four TRXs, two CBSXs and AMP, the mean is
573 defined as the single TRX, CBSX and AMP effects, their pairwise interactions and the third
574 order interaction.
575 For the DMC-MDH activities dataset, the mean is defined as the single TRX, CBSX and
576 AMP effects and the interaction between CBSX and TRX. This model is the most complete
577 according to the experimental design.
578 For the MDH activities dataset with AMP, ATP and MgATP, the mean is defined as the
579 single CBSX and ligand effects and their interaction.
580 For MDH activities dataset with AMP, ADP and ATP, the mean is defined as the single
581 CBSX and ligand effects and their interaction.
582 For the MDH activities dataset with AMP and ATP ranging from 1µM to 1mM, the mean is
583 defined as the single CBSX and ligand effects and their interaction.

For the PRX activities dataset with CBSX2 and AMP effects on TRX m1 (Figure 7), the mean is defined as the single CBSX and AMP effects and their interaction.

For the rosette fresh-weight and chlorophyll content datasets, the mean is defined as the genotype effect.

For *in planta* MDH initial and maximal activities dataset, the mean is defined as the genotype effect.

Pull-down

Purified 6His-CBSX2 protein (500 µg) was incubated with TRX m1 (285 µg) in 350 µL assay buffer (1x PBS, ± 1 mM DTE ± 1 mM AMP ± 1 mM ATP) for 1h at room temperature. After adding 50 µL of Ni-NTA agarose beads (Qiagen) and incubation for 1h at room temperature, beads were washed 3 times with 500 µL of assay buffer. Proteins were eluted with 200 mM imidazole. Immunoblotting was performed with mouse anti-6HIS (Roche® #11922416001) and rabbit specific anti-TRXm1 (generated against AtTRXm1 recombinant protein, Genosphere Biotechnologies) as primary antibodies, and anti-mouse (Sigma A5906) and anti-rabbit (Sigma A6154) as HRP-conjugated secondary antibodies. Blot revelation was performed with the BIORAD Clarity™ Western ECL Substrate on a BIORAD® Chemidoc ISV0025.

ACCESSION NUMBERS

CBSX1 (AT4G36910), *CBSX2* (AT4G34120), *CBSX3* (AT5G10860), *CBSX4* (AT1G80090), *CBSX5* (AT4G27460), *CBSX6* (AT1G65320), *TRXM1* (AT1G03680), *TRXM2* (AT4G03520), *TRXF1* (AT3G02730), *TRXF2* (AT5G16400), *TRXX* (AT1G50320), *TRXY1* (AT1G76760), *NUWA* (AT3G49240) and *DYW2* (AT2G15690).

2-CYS PRXA (AT5G58330), *NADP-MDH* (AT3G11630).

SUPPLEMENTAL MATERIAL

Table S1: Primer used

Figure S1: *Arabidopsis thaliana* CBSX phylogenetic tree.

Figure S2: Subcellular localization of CBSX1, CBSX2 and CBSX3.

Figure S3: NADP-MDH activation kinetics.

Figure S4: Test of direct effect of adenylates on TRXm1 dependent NADP-MDH activation.

Figure S5: Effect of AMP on mutant DMC-MDH activity.

Figure S6: Effect of ATP on CBSX2 towards TRXm1-dependent NADP-MDH activation.
Figure S7: Effects of ATP together with ADP at concentrations and ratios mimicking light and night conditions, on CBSX2 towards TRXm1-dependent NADP-MDH activation.
Figure S8: TRX targets in the context of CBSX mutations.
Figure S9: P700+ reduction.

ACKNOWLEDGMENTS

We greatly thank Marie-Laure Martin-Magniette who helped us for statistical analysis. We are grateful to Cécile Raynaud who provided us with the *Agrobacterium* strain containing the HC-pro silencing inhibitor. We would also like to thank Myroslawa Miginiac-Maslow for constructive criticism of the manuscript.

FIGURE LEGENDS

Figure 1. Protein interactions between Arabidopsis CBSX isoforms assayed by yeast 2-hybrid.

Interactions were tested using a mating-based Y2H matricial assay with AD fusions on the horizontal axis and the DB fusions on the vertical axis. In the "H2O" row and column, yeast cells were replaced by water; in the "Ø" row and column, mating was performed with yeasts transformed with an empty vector. As a positive interaction control, we used DB-mNUWA and AD-mDYW2 (Guillaumot et al., 2017). Interactions were tested on selective medium without histidine.

Figure 2. *In planta* protein interactions between CBSX isoforms assayed by BiFC.

BiFC of YFP in transiently transformed Nicotiana benthamiana leaves. Left column, YFP fluorescence signal. Middle column, chlorophyll fluorescence signal. Right column, merge of fluorescent signals. Fluorescence spots confirmed as YFP fluorescence signals by spectral analysis are indicated by white arrows. Observations were performed four days after transformations. Bars=10 µm.

Figure 3. Effect of CBSX1 and 2 on TRX capacity to activate wild-type NADP-MDH, and effect of AMP.

NADP-MDH activation was measured after 20 min incubation at room temperature in presence of 10 µM TRX (except TRXf1 at 1 µM) and 10 mM DTE. 100% activation rate corresponds to the activation with DTE-reduced TRX (without CBSX and AMP). (A) TRXm1 (mean SA = 372 u/mg), (B) TRXm2 (mean SA = 314 u/mg), (C) TRXm4 (mean SA = 383 u/mg), (D) TRXf1 (mean SA = 432 u/mg) and (E) TRXf2 (mean SA = 340 u/mg).

648 CBSX1/2 and AMP final concentration were 30 µM and 1 mM, respectively. Values are
649 means ± SD (n=4). Bars with different letters correspond to significantly different values. $P <$
650 0.05. SA: specific activity of NADP-MDH at maximal activation (100%) expressed in units
651 (u: µmole NADPH oxidized per min) per mg of enzyme.
652 **Figure 4.** Effect of CBSX2 on mutant DMC-MDH activity and TRXm-dependent activation,
653 and effect of AMP.
654 DMC-MDH activation was measured after 20 min incubation at room temperature in presence
655 of DTE alone (Ø TRX) or DTE + TRXm1 or DTE + TRXm2. 100% activation rate
656 corresponds to the maximal activation of DMC-MDH by DTE-reduced TRXm1/2 (without
657 CBSX and AMP). Mean specific activity of DMC-MDH at maximal activation (100%) were
658 391 u/mg and 382 u/mg, with TRXm1 and TRXm2, respectively. Values are means ± SD
659 (n=4). TRXm1/2, CBSX2 and AMP were at a final concentration of 10 µM, 30 µM and 1
660 mM, respectively. Bars with different letters correspond to significantly different values. $P <$
661 0.05.
662 **Figure 5.** Effects of adenylates on CBSX2 inhibition of TRXm-dependent NADP-MDH
663 activation.
664 Wild-type MDH activation was measured after 20 min incubation in presence of DTE-
665 reduced TRXm1 (10 µM) with CBSX2 (30 µM) and 0, 1, 10, 50 or 1000 µM of AMP, ADP
666 or ATP. Values are means ± SD (n=4-6). Bars with different letters correspond to
667 significantly different values. $P < 0.05$.
668 **Figure 6.** Effect of CBSX1 and 2 on 2-Cys PRX activity.
669 Time course of tBOOH reduction by 2-Cys PRXA was quantified by the FOX assay in
670 presence of DTT alone (black curves), DTT-reduced TRX (grey curves), DTT-reduced TRX
671 and CBSX1 (blue curves) or DTT-reduced TRX and CBSX2 (orange curves). (A) DTT alone;
672 (B) DTT + TRX x; (C) DTT + TRX f1; (D) DTT + TRX y1; (E) DTT + TRX m1; (F) DTT +
673 NTRC. The values are means ± SD (n=3).
674 **Figure 7.** Effect of 1 mM AMP on CBSX2 towards TRXm1-dependent 2-Cys PRX activity.
675 2-Cys PRX activities were defined as the tBOOH reduction kinetic slope between 2 and 10
676 min and were normalized to the activity in the control condition (without CBSX and AMP)
677 considered as 100%. The values are means ± SD (n=3). Bars with different letters correspond
678 to significantly different values. $P < 0.05$.
679 **Figure 8.** Pull-down assays with CBSX and TRXm proteins.
680 Pull-down of His-CBSX and TRXm1 in absence or presence of DTE, AMP and ATP. (A)
681 Impact of 1 mM AMP and DTE on CBSX2-TRXm1 interaction. (B) Impact of 1 mM ATP or

682 1 mM AMP on CBSX-TRXm1 interaction. Input corresponds to proteins initially mixed
683 before incubation with His-affinity agarose beads. Output corresponds to proteins eluted (after
684 washes) from the resin by 200 mM imidazole. The bracket indicates an unspecific low
685 molecular weight signal obtained using anti-TRX m1 antibodies on CBSX preparations.
686 **Figure 9.** *cbsx* mutant phenotypes.
687 (A) Representative 5-week old plants grown in long day conditions at 20°C (bar= 1cm). (B)
688 Representative 11-week old plants grown in long day conditions at 12°C (bar= 1cm). (C) and
689 (D) Plants grown at control temperature. (E) and (F) Plants grown at low temperature. (C) and
690 (E) Rosette fresh weight, values are means ± SD (n=10), *: $P < 0.01$. (D) and (F) Chlorophyll
691 a and b contents, and Chla/Chlb ratios, values are means ± SD (n=10). *: $P = 0.02$.
692 **Figure 10.** P700 measurements on leaves of wild-type plants and Trx m and CBSX-deficient
693 mutants.
694 The redox state of the PSI primary donor P700 was monitored through the changes in
695 absorbance at 830 versus 875 nm. (A) Representative curves are shown of plants kept at
696 growth light intensity; WT: black, *cbsx1cbsx2*: red, *trxm1trxm2*: green. Leaves were
697 illuminated with actinic red light, AL (I=830 µmol photons.m^{-2}.s^{-1}) to oxidize P700 until a
698 steady state was reached. Then far-red light, FR, was switched on. To achieve the maximum
699 oxidation state a saturating flash, SF, was given at the end of the FR illumination. (B) Half-
700 time of P700+ reduction after FR illumination of dark-adapted plants. The traces of the
701 kinetics are shown in Figure S9. Bars with different letters correspond to significantly
702 different values between genotypes. $P < 0.05$.
703 **Figure 11.** Model of TRX activity regulation by CBSX2.
704 CBSX2 homodimer (yellow disc) is unable to interact with oxidized TRX m (green circle)
705 (A), but is able to interact with reduced TRXm and inhibits TRX m capacity to reduce its
706 target (blue circle) (B). A conformational change of CBSX2 induced by adenosyl ligand (red
707 circle) binding provokes the release of TRXm-CBSX2 interaction allowing TRX m to act on
708 its target (C).
709 **Figure 12.** Model for functional relationship between CBSX and TRX in the context of ATP
710 homeostasis in the chloroplast.
711 In the proposed model, when ATP level is low (A), CBSX can interact with TRX m impeding
712 its negative regulation towards PSI-CET, primarily coupled to the generation of the proton
713 motive force driving the synthesis of ATP by the thylakoid ATP synthase complex. When
714 ATP level increases (B), ATP binds to CBSX which cannot interact with TRX m, allowing
715 down-regulation of the PSI-CET and thereby lowering ATP synthesis.

716 Electron and proton transfers are shown by red and blue arrows, respectively. Abbreviations
717 are : PSI/II, photosystem I/II; Cyt b6/f, cytochrome b6/f complex; Fd, ferredoxin; FNR,
718 ferredoxin-NADP reductase; FTR, ferredoxin/thioredoxin reductase; TRX, thioredoxin;
719 CBSX, Cystathionine-β-synthase containing domain protein; PQ, plastoquinone; PQH2,
720 plastoquinol; PC, plastocyanin; PSI-CET, cyclic electron transport around PSI.

721

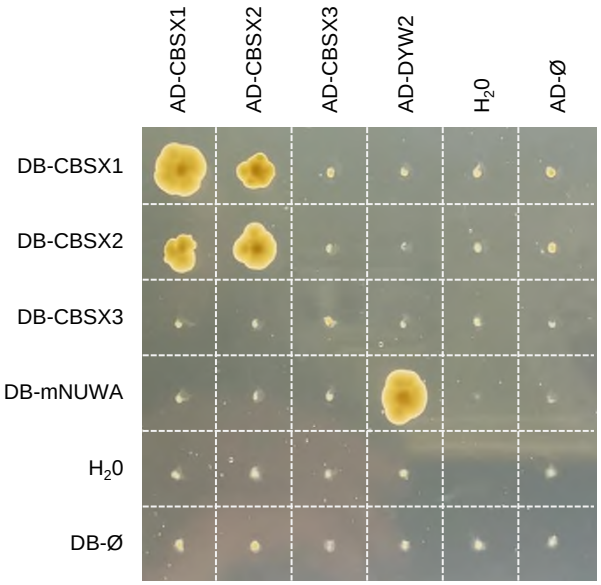

Figure 1. Protein interactions between Arabidopsis CBSX isoforms assayed by yeast 2-hybrid.

Interactions were tested using a mating-based Y2H matricial assay with AD fusions on the horizontal axis and the DB fusions on the vertical axis. In the “H2O” row and column, yeast cells were replaced by water; in the “Ø” row and column, mating was performed with yeasts transformed with an empty vector. As a positive interaction control, we used DB-mNUWA and AD-mDYW2 (Guillaumot et al., 2017). Interactions were tested on selective medium without histidine.

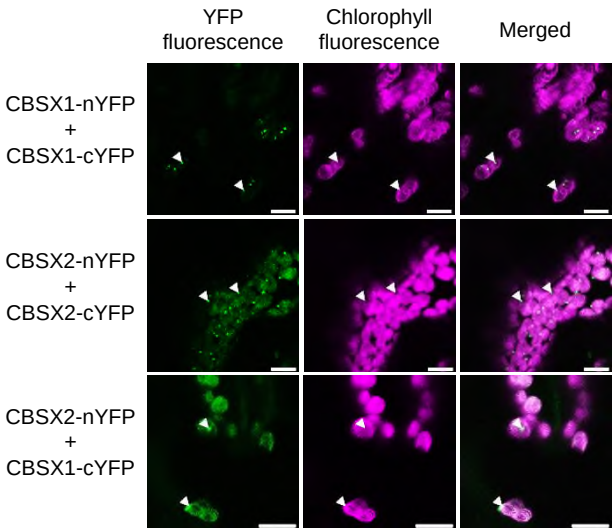

Figure 2. *In planta* protein interactions between CBSX isoforms assayed by BiFC.

BiFC of YFP in transiently transformed *Nicotiana benthamiana* leaves. Left column, YFP fluorescence signal. Middle column, chlorophyll fluorescence signal. Right column, merge of fluorescent signals. Fluorescence spots confirmed as YFP fluorescence signals by spectral analysis are indicated by white arrows. Observations were performed four days after transformations. Bars=10 µm.

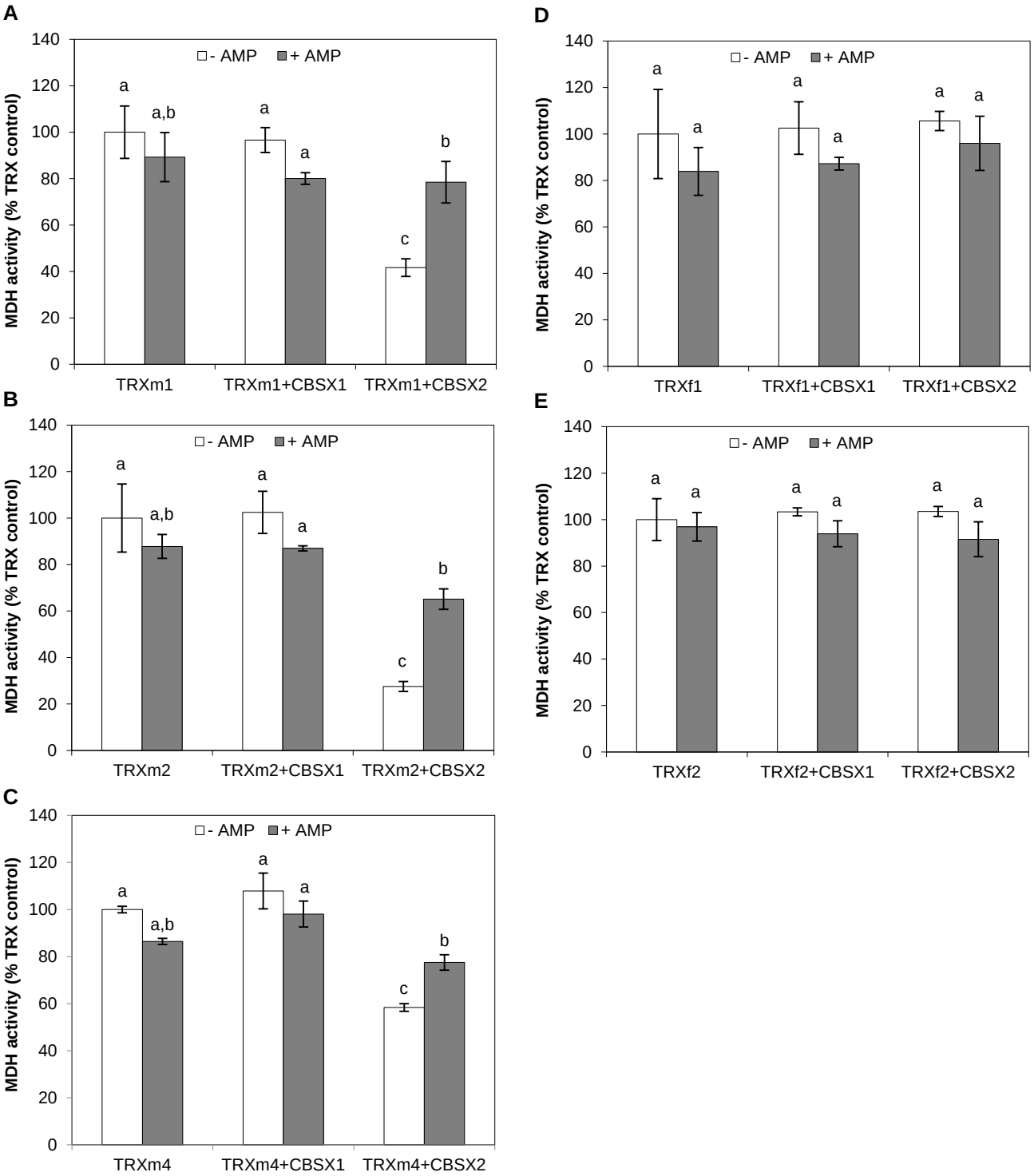

Figure 3. Effect of CBSX1 and 2 on TRX capacity to activate wild-type NADP-MDH, and effect of AMP.

NADP-MDH activation was measured after 20 min incubation at room temperature in presence of 10 µM TRX (except TRXf1 at 1 µM) and 10 mM DTE. 100% activation rate corresponds to the activation with DTE-reduced TRX (without CBSX and AMP). (A) TRXm1 (mean SA = 372 u/mg), (B) TRXm2 (mean SA = 314 u/mg), (C) TRXm4 (mean SA = 383 u/mg), (D) TRXf1 (mean SA = 432 u/mg) and (E) TRXf2 (mean SA = 340 u/mg). CBSX1/2 and AMP final concentration were 30 µM and 1 mM, respectively. Values are means ± SD (n=4). Bars with different letters correspond to significantly different values. $P < 0.05$. SA: specific activity of NADP-MDH at maximal activation (100%) expressed in units (u: µmole NADPH oxidized per min) per mg of enzyme.

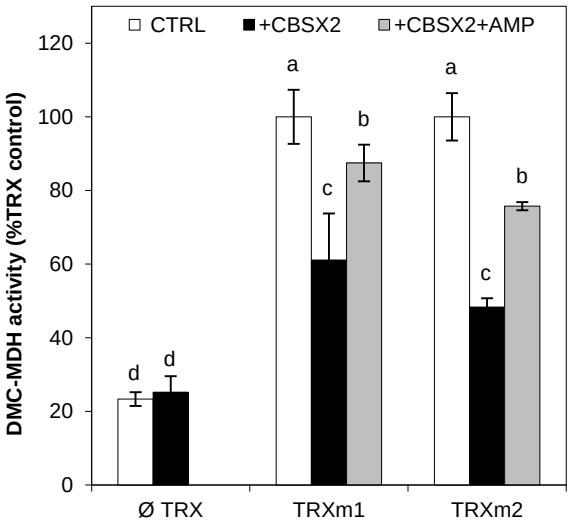

Figure 4. Effect of CBSX2 on mutant DMC-MDH activity and TRXm-dependent activation, and effect of AMP.

DMC-MDH activation was measured after 20 min incubation at room temperature in presence of DTE alone (Ø TRX) or DTE + TRXm1 or DTE + TRXm2. 100% activation rate corresponds to the maximal activation of DMC-MDH by DTE-reduced TRXm1/2 (without CBSX and AMP). Mean specific activity of DMC-MDH at maximal activation (100%) were 391 u/mg and 382 u/mg, with TRXm1 and TRXm2, respectively. Values are means ± SD (n=4). TRXm1/2, CBSX2 and AMP were at a final concentration of 10 µM, 30 µM and 1 mM, respectively. Bars with different letters correspond to significantly different values. $P < 0.05$.

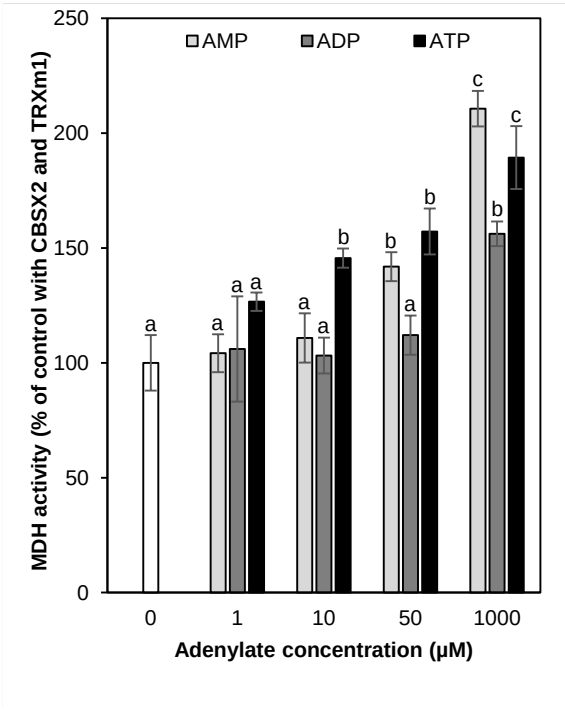

Figure 5. Effects of adenylates on CBSX2 inhibition of TRXm-dependent NADP-MDH activation.

Wild-type MDH activation was measured after 20 min incubation in presence of DTE-reduced TRXm1 (10 µM) with CBSX2 (30 µM) and 0, 1, 10, 50 or 1000 µM of AMP, ADP or ATP. Values are means ± SD (n=4-6). Bars with different letters correspond to significantly different values. $P < 0.05$.

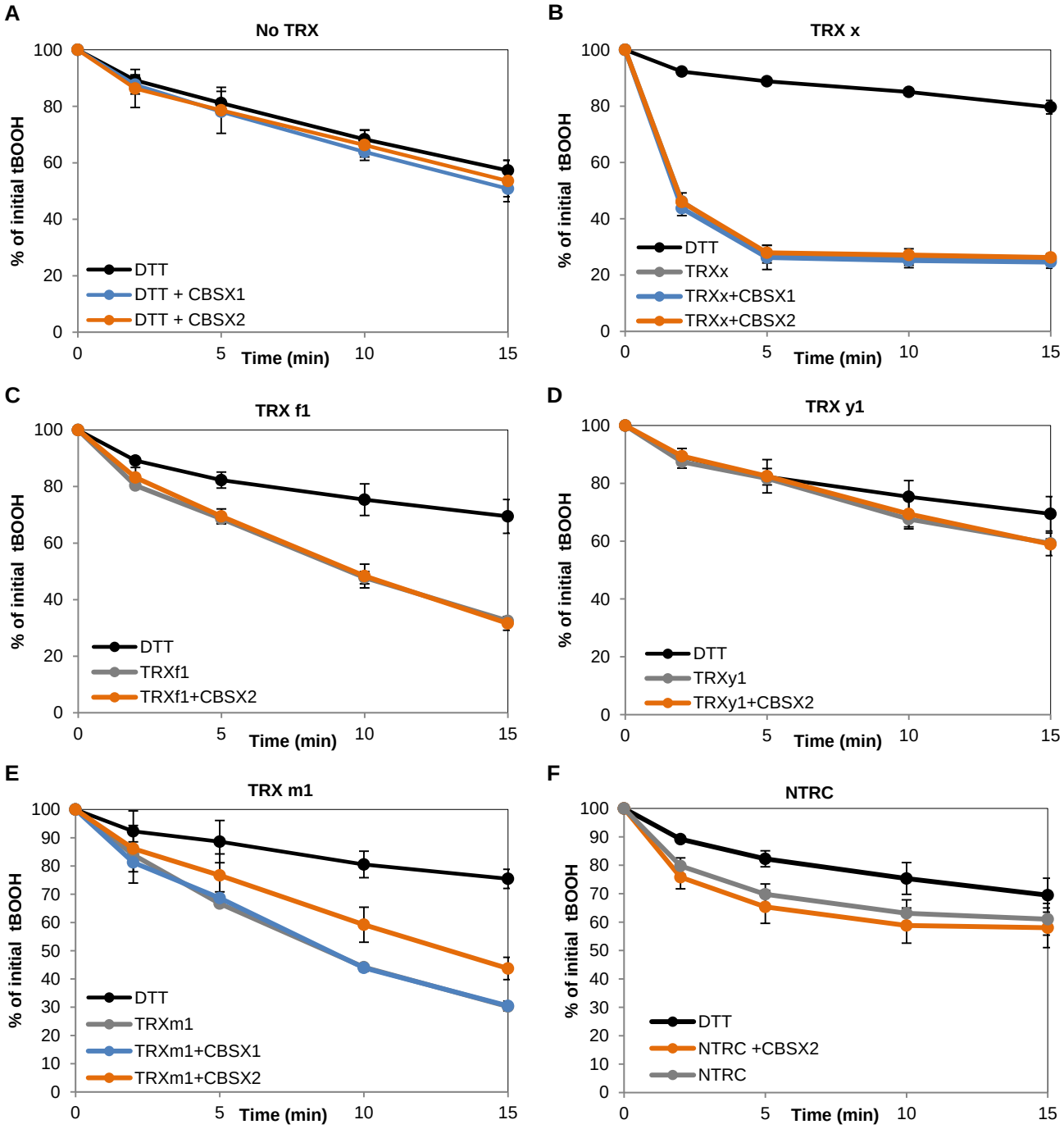

Figure 6. Effect of CBSX1 and 2 on 2-Cys PRX activity.

Time course of tBOOH reduction by 2-Cys PRXA was quantified by the FOX assay in presence of DTT alone (black curves), DTT-reduced TRX (grey curves), DTT-reduced TRX and CBSX1 (blue curves) or DTT-reduced TRX and CBSX2 (orange curves). (A) DTT alone; (B) DTT + TRX x; (C) DTT + TRX f1; (D) DTT + TRX y1; (E) DTT + TRX m1; (F) DTT + NTRC. The values are means ± SD (n=3).

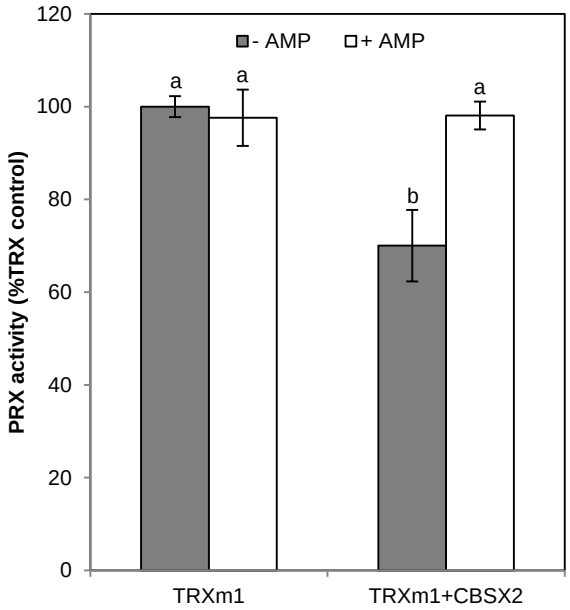

Figure 7. Effect of 1 mM AMP on CBSX2 towards TRXm1-dependent 2-Cys PRX activity.

2-Cys PRX activities were defined as the tBOOH reduction kinetic slope between 2 and 10 min and were normalized to the activity in the control condition (without CBSX and AMP) considered as 100%. The values are means ± SD (n=3). Bars with different letters correspond to significantly different values. $P < 0.05$.

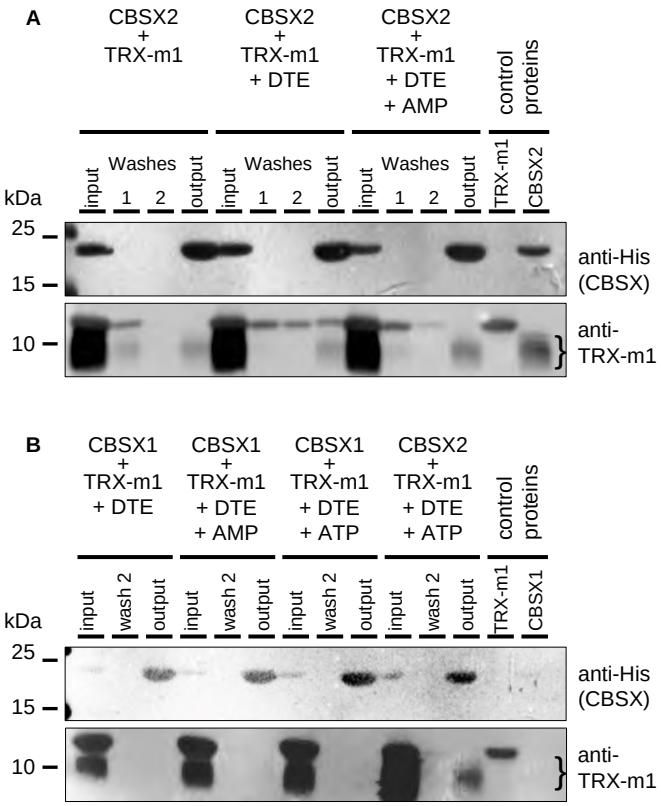

Figure 8. Pull-down assays with CBSX and TRXm proteins.

Pull-down of His-CBSX and TRXm1 in absence or presence of DTE, AMP and ATP. (A) Impact of 1 mM AMP and DTE on CBSX2-TRXm1 interaction. (B) Impact of 1 mM ATP or 1 mM AMP on CBSX-TRXm1 interaction. Input corresponds to proteins initially mixed before incubation with His-affinity agarose beads. Output corresponds to proteins eluted (after washes) from the resin by 200 mM imidazole. The bracket indicates an unspecific low molecular weight signal obtained using anti-TRX m1 antibodies on CBSX preparations.

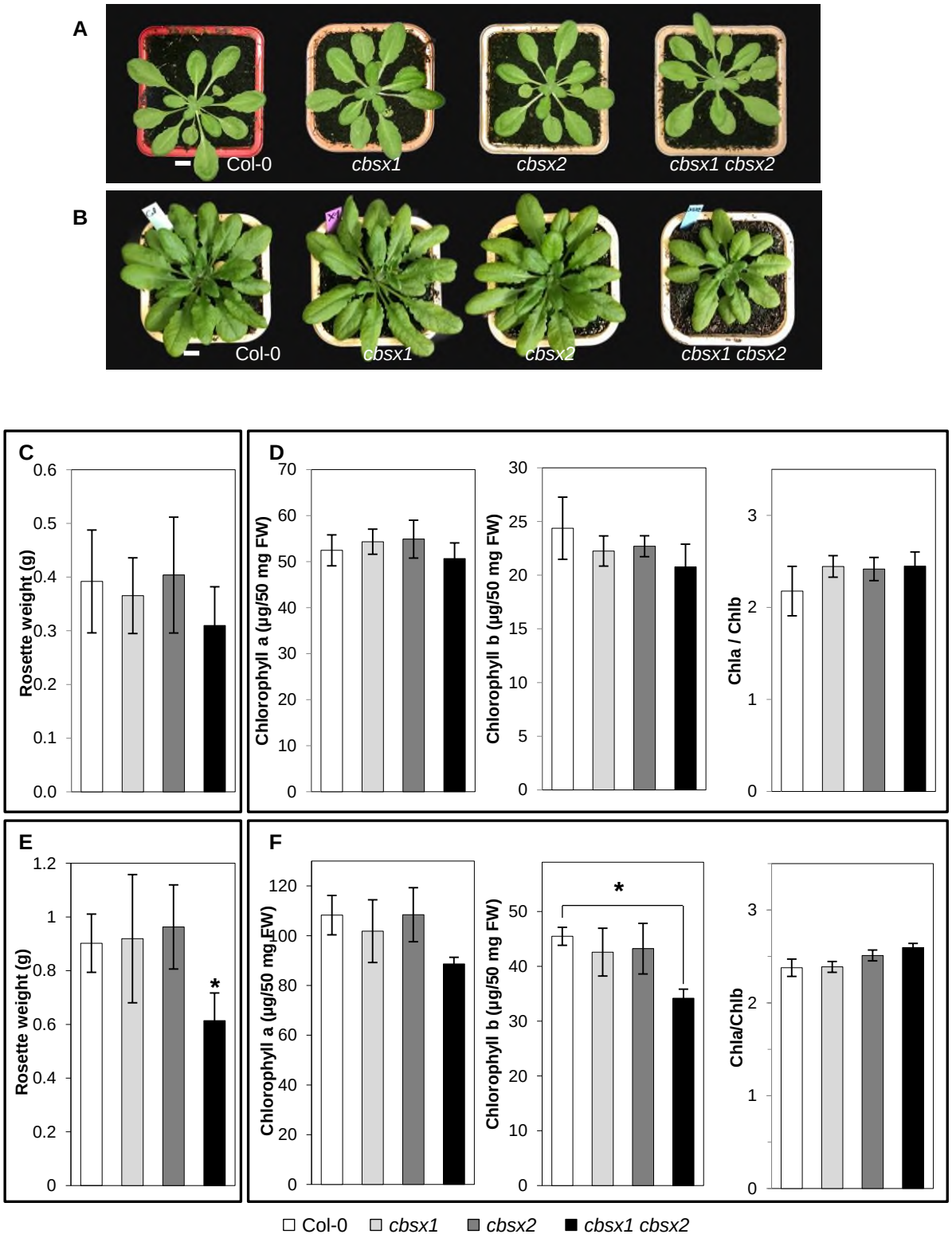

Figure 9. *cbsx* mutant phenotypes.

(A) Representative 5-week old plants grown in long day conditions at 20°C (bar = 1 cm). (B) Representative 11-week old plants grown in long day conditions at 12°C (bar = 1 cm). (C) and (D) Plants grown at control temperature. (E) and (F) Plants grown at low temperature. (C) and (E) Rosette fresh weight, values are means ± SD (n=10), *: $P < 0.01$. (D) and (F) Chlorophyll a and b contents, and Chla/Chlb ratios, values are means ± SD (n=10). *: $P = 0.02$.

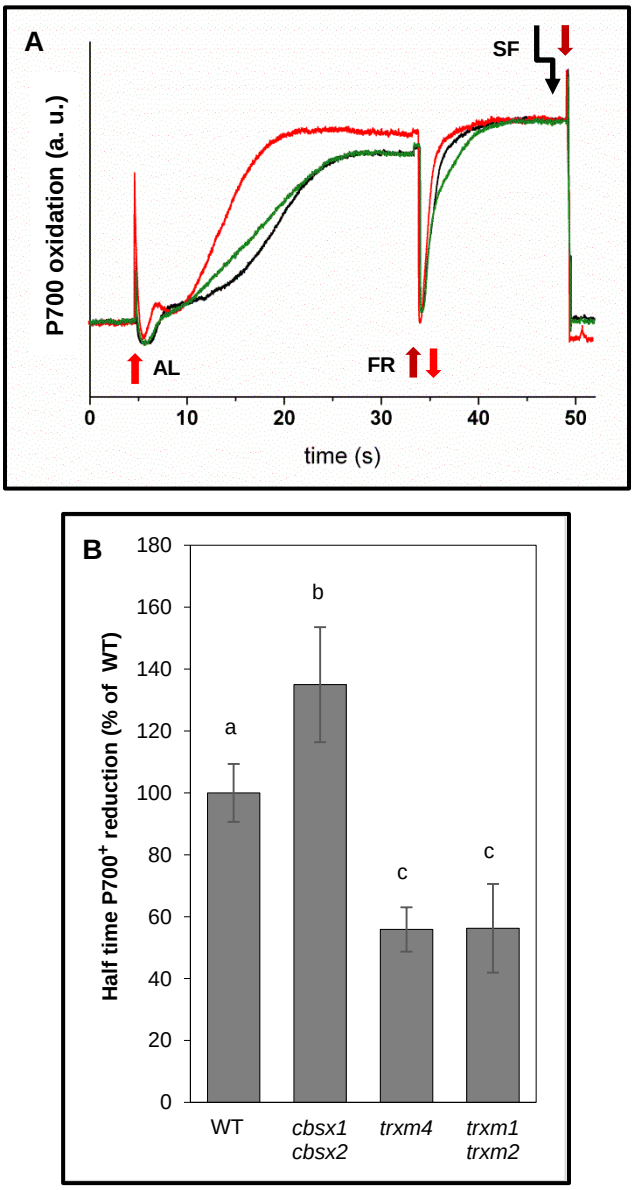

Figure 10. P700 measurements on leaves of wild-type plants and Trx m and CBSX-deficient mutants.

The redox state of the PSI primary donor P700 was monitored through the changes in absorbance at 830 versus 875 nm. (A) Representative curves are shown of plants kept at growth light intensity; WT: black, *cbsx1cbsx2*: red, *trxm1trxm2*: green. Leaves were illuminated with actinic red light, AL (I = 830 µmol photons.m^{-2}.s^{-1}) to oxidize P700 until a steady state was reached. Then far-red light, FR, was switched on. To achieve the maximum oxidation state a saturating flash, SF, was given at the end of the FR illumination. (B) Half-time of $P700^+$ reduction after FR illumination of dark-adapted plants. The traces of the kinetics are shown in Figure S9. Bars with different letters correspond to significantly different values between genotypes. $P < 0.05$.

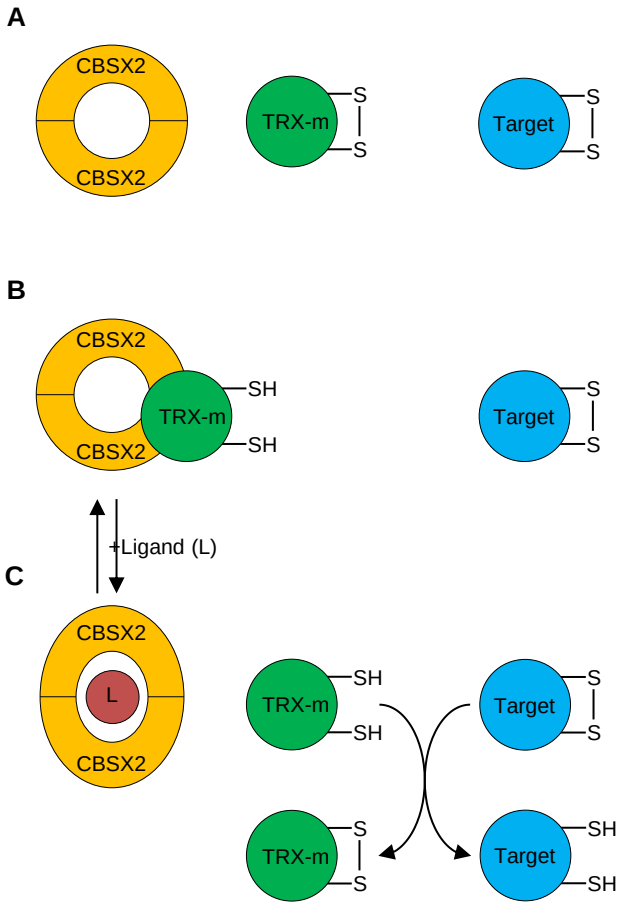

Figure 11. Model of TRX activity regulation by CBSX2.

CBSX2 homodimer (yellow disc) is unable to interact with oxidized TRX m (green circle) (A), but is able to interact with reduced TRXm and inhibits TRX m capacity to reduce its target (blue circle) (B). A conformational change of CBSX2 induced by adenosyl ligand (red circle) binding provokes the release of TRXm-CBSX2 interaction allowing TRX m to act on its target (C).

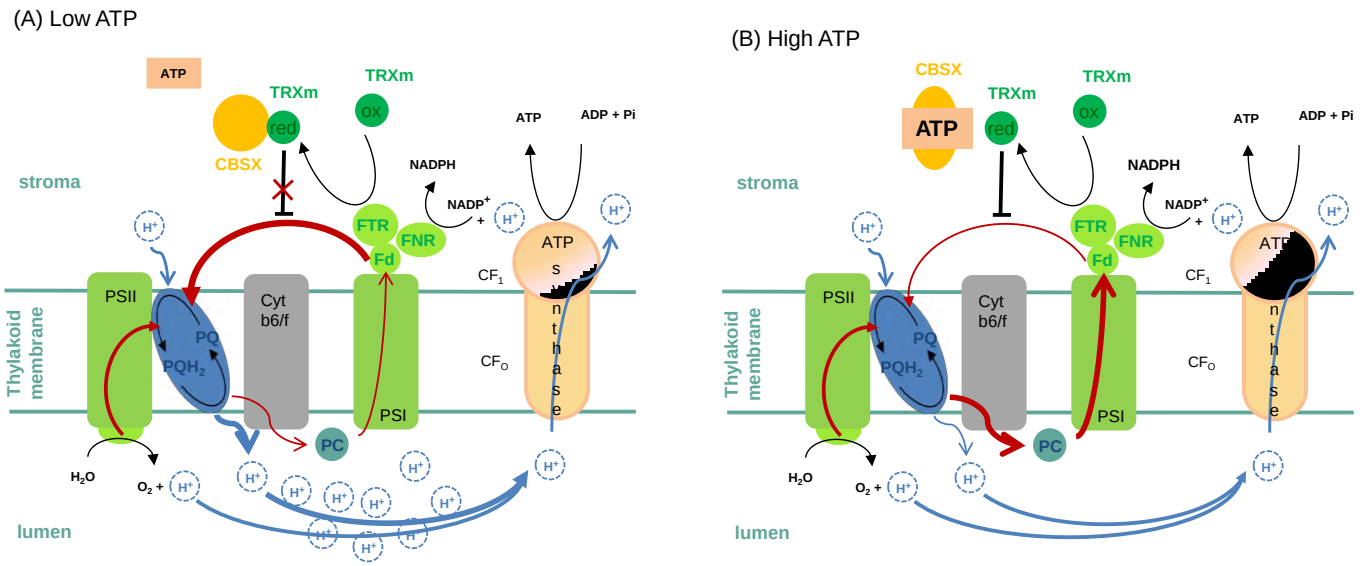

Figure 12. Model for functional relationship between CBSX and TRX in the context of ATP homeostasis in the chloroplast.

In the proposed model, when ATP level is low (A), CBSX can interact with TRX m impeding its negative regulation towards PSI-CET, primarily coupled to the generation of the proton motive force driving the synthesis of ATP by the thylakoid ATP synthase complex. When ATP level increases (B), ATP binds to CBSX which cannot interact with TRX m, allowing down-regulation of the PSI-CET and thereby lowering ATP synthesis.
Electron and proton transfers are shown by red and blue arrows, respectively. Abbreviations are : PSI/II, photosystem I/II; Cyt b6/f, cytochrome b6/f complex; Fd, ferredoxin; FNR, ferredoxin-NADP reductase; FTR, ferredoxin/thioredoxin reductase; TRX, thioredoxin; CBSX, Cystathionine-β-synthase containing domain protein; PQ, plastoquinone; PQH2, plastoquinol; PC, plastocyanin; PSI-CET, cyclic electron transport around PSI.

Parsed Citations

Baier M, Dietz K-J (2005) Chloroplasts as source and target of cellular redox regulation: a discussion on chloroplast redox signals in the context of plant physiology. J Exp Bot 56: 1449–1462
Google Scholar: Author Only Title Only Author and Title

Bateman A (1997) The structure of a domain common to archaebacteria and the homocystinuria disease protein. Trends Biochem Sci. doi: 10.1016/S0968-0004(96)30046-7
Google Scholar: Author Only Title Only Author and Title

Bohrer A-S, Massot V, Innocenti G, Reichheld J-P, Issakidis-Bourguet E, Vanacker H (2012) New insights into the reduction systems of plastidial thioredoxins point out the unique properties of thioredoxin z from Arabidopsis. J Exp Bot 63: 6315–6323
Google Scholar: Author Only Title Only Author and Title

Boussardon C, Salone V, Avon A, Berthome R, Hammani K, Okuda K, Shikanai T, Small I, Lurin C (2012) Two interacting proteins are necessary for the editing of the NdhD-1 Site in Arabidopsis plastids. Plant Cell 24: 3684–3694
Google Scholar: Author Only Title Only Author and Title

Buey RM, Fernández-Justel D, Marcos-Alcalde Í, Winter G, Gómez-Puertas P, de Pereda JM, Luis Revuelta J (2017) A nucleotide-controlled conformational switch modulates the activity of eukaryotic IMP dehydrogenases. Sci Rep 7: 2648
Google Scholar: Author Only Title Only Author and Title

Collin V, Issakidis-Bourguet E, Marchand C, Hirasawa M, Lancelin J-M, Knaff DB, Miginiac-Maslow M (2003) The Arabidopsis plastidial thioredoxins: new functions and new insights into specificity. J Biol Chem 278: 23747–23752
Google Scholar: Author Only Title Only Author and Title

Collin V, Lamkemeyer P, Miginiac-Maslow M, Hirasawa M, Knaff DB, Dietz K-J, Issakidis-Bourguet E (2004) Characterization of plastidial thioredoxins from Arabidopsis belonging to the new y-type. Plant Physiol 136: 4088–4095
Google Scholar: Author Only Title Only Author and Title

Cornic G, Bukhov NG, Wiese C, Bligny R, Heber U (2000) Flexible coupling between light-dependent electron and vectorial proton transport in illuminated leaves of C3 plants. Role of photosystem I-dependent proton pumping. Planta 210: 468–477
Google Scholar: Author Only Title Only Author and Title

Courteille A, Vesa S, Sanz-Barrio R, Cazale A-C, Becuwe-Linka N, Farran I, Havaux M, Rey P, Rumeau D (2013) Thioredoxin m4 Controls Photosynthetic Alternative Electron Pathways in Arabidopsis. Plant Physiol 161: 508–520
Google Scholar: Author Only Title Only Author and Title

Crozet P, Margalha L, Confraria A, Rodrigues A, Martinho C, Adamo M, Elias CA, Baena-González E (2014) Mechanisms of regulation of SNF1/AMPK/SnRK1 protein kinases. Front Plant Sci. doi: 10.3389/fpls.2014.00190
Google Scholar: Author Only Title Only Author and Title

Da Q, Sun T, Wang M, Jin H, Li M, Feng D, Wang J, Wang H-B, Liu B (2017) M-type thioredoxins are involved in the xanthophyll cycle and proton motive force to alter NPQ under low-light conditions in Arabidopsis. Plant Cell Rep 37: 279–291
Google Scholar: Author Only Title Only Author and Title

Dreyer A, Dietz K-J (2018) Reactive Oxygen Species and the Redox-Regulatory Network in Cold Stress Acclimation. Antioxidants 7: 169
Google Scholar: Author Only Title Only Author and Title

Dreze M, Monachello D, Lurin C, Cusick ME, Hill DE, Vidal M, Braun P (2010) High-quality binary interactome mapping. Methods Enzymol. doi: 10.1016/S0076-6879(10)70012-4
Google Scholar: Author Only Title Only Author and Title

Emanuelsson O, Nielsen H, Brunak S, von Heijne G (2000) Predicting Subcellular Localization of Proteins Based on their N-terminal Amino Acid Sequence. J Mol Biol 300: 1005–1016
Google Scholar: Author Only Title Only Author and Title

Ereño-Orbea J, Oyenarte I, Martínez-Cruz LA (2013) CBS domains: Ligand binding sites and conformational variability. Arch Biochem Biophys. doi: 10.1016/j.abb.2013.10.008
Google Scholar: Author Only Title Only Author and Title

Fang L, Hou X, Lee LYC, Liu L, Yan X, Yu H (2011) AtPV42a and AtPV42b redundantly regulate reproductive development in arabidopsis thaliana. PLoS One 6: 21–23
Google Scholar: Author Only Title Only Author and Title

Fisher N, Bricker TM, Kramer DM (2019) Regulation of photosynthetic cyclic electron flow pathways by adenylate status in higher plant chloroplasts. Biochim Biophys Acta - Bioenerg 1860: 148081
Google Scholar: Author Only Title Only Author and Title

Geigenberger P, Thormählen I, Daloso DM, Fernie AR (2017) The unprecedented versatility of the plant thioredoxin system. Trends Plant Sci 22: 249–262
Google Scholar: Author Only Title Only Author and Title

Gelhaye E, Rouhier N, Navrot N, Jacquot JP (2005) The plant thioredoxin system. Cell Mol Life Sci 62: 24–35
Google Scholar: Author Only Title Only Author and Title

Guillaumot D, Lopez-Obando M, Baudry K, Avon A, Rigaill G, Falcon de Longevialle A, Broche B, Takenaka M, Berthomé R, De Jaeger G, et al (2017) Two interacting PPR proteins are major Arabidopsis editing factors in plastid and mitochondria. Proc Natl Acad Sci 114: 201705780
Google Scholar: Author Only Title Only Author and Title

Hardie DG, Hawley S a. (2001) AMP-activated protein kinase: The energy charge hypothesis revisited. BioEssays 23: 1112–1119
Google Scholar: Author Only Title Only Author and Title

Hertle AP, Blunder T, Wunder T, Pesaresi P, Pribil M, Armbruster U, Leister D (2013) PGRL1 is the elusive ferredoxin-plastoquinone reductase in photosynthetic cyclic electron flow. Mol Cell 49: 511–523
Google Scholar: Author Only Title Only Author and Title

Ignoul S, Eggermont J (2005) CBS domains: structure, function, and pathology in human proteins. Am J Physiol Physiol 289: C1369–C1378
Google Scholar: Author Only Title Only Author and Title

Issakidis E, Saarinen M, Decottignies P, Jacquot J, Crétin C, Gadal P, Miginiac-Maslow M (1994) Identification and characterization of second regulatory disulfide bridge of recombinant Sorghum leaf NADP-Malate Dehydrogenase. J. Biol. Chem. 269:
Google Scholar: Author Only Title Only Author and Title

James P, Halladay J, Craig EA (1996) Genomic libraries and a host strain designed for highly efficient two-hybrid selection in yeast. Genetics 144: 1425–36
Google Scholar: Author Only Title Only Author and Title

Jeong B-C, Park SH, Yoo KS, Shin JS, Song HK (2013a) Change in single cystathionine β-synthase domain-containing protein from a bent to flat conformation upon adenosine monophosphate binding. J Struct Biol 183: 40–46
Google Scholar: Author Only Title Only Author and Title

Jeong B-C, Park SH, Yoo KS, Shin JS, Song HK (2013b) Crystal structure of the single cystathionine β-synthase domain-containing protein CBSX1 from Arabidopsis thaliana. Biochem Biophys Res Commun 430: 265–271
Google Scholar: Author Only Title Only Author and Title

Jones DT, Taylor WR, Thornton JM (1992) The rapid generation of mutation data matrices from protein sequences. Comput Appl Biosci 8: 275–82
Google Scholar: Author Only Title Only Author and Title

Junesch U, Gräber P (1987) The activation of the reduced chloroplast ATP-synthase by ΔpH. Prog. Photosynth. Res. Springer Netherlands, Dordrecht, pp 173–176
Google Scholar: Author Only Title Only Author and Title

Jung KW, Kim YY, Yoo KS, Ok SH, Cui MH, Jeong BC, Yoo SD, Jeung JU, Shin JS (2013) A cystathionine-b-synthase domain-containing protein, CBSX2, regulates endothecial secondary cell wall thickening in anther development. Plant Cell Physiol. doi: 10.1093/pcp/pcs166
Google Scholar: Author Only Title Only Author and Title

Kemp BE (2004) Bateman domains and adenosine derivatives form a binding contract. J Clin Invest 113: 182–184
Google Scholar: Author Only Title Only Author and Title

Kobayashi Y, Inoue Y, Furuya F, Shibata K, Heber U (1979) Regulation of adenylate levels in intact spinach chloroplasts. Planta 147: 69–75
Google Scholar: Author Only Title Only Author and Title

Kumar S, Stecher G, Tamura K (2016) MEGA7: Molecular evolutionary genetics analysis Version 7.0 for bigger datasets. Mol Biol Evol 33: 1870–1874
Google Scholar: Author Only Title Only Author and Title

Kushwaha HR, Singh AK, Sopory SK, Singla-Pareek SL, Pareek A (2009) Genome wide expression analysis of CBS domain containing proteins in Arabidopsis thaliana L. and Oryza sativa L. reveals their developmental and stress regulation. BMC Genomics 10: 200
Google Scholar: Author Only Title Only Author and Title

Lemaire SD, Michelet L, Zaffagnini M, Massot V, Issakidis-Bourguet E (2007) Thioredoxins in chloroplasts. Curr Genet 51: 343–365

Google Scholar: Author Only Title Only Author and Title

Michelet L, Zaffagnini M, Marchand C, Collin V, Decottignies P, Tsan P, Lancelin J-M, Trost P, Miginiac-Maslow M, Noctor G, et al (2005) Glutathionylation of chloroplast thioredoxin f is a redox signaling mechanism in plants. Proc Natl Acad Sci 102: 16478–16483
Google Scholar: Author Only Title Only Author and Title

Miyake C (2020) Molecular mechanism of oxidation of P700 and suppression of ROS production in Photosystem I in response to electron-sink limitations in C3 plants. Antioxidants 9: 230
Google Scholar: Author Only Title Only Author and Title

Monachello D, Guillaumot D, Lurin C (2019) A pipeline for systematic yeast 2-hybrid matricial screening in liquid culture. Protoc Exch. doi: 10.21203/rs.2.9948/v1
Google Scholar: Author Only Title Only Author and Title

Montrichard F, Alkhalfioui F, Yano H, Vensel WH, Hurkman WJ, Buchanan BB (2009) Thioredoxin targets in plants: The first 30 years. J Proteomics 72: 452–474
Google Scholar: Author Only Title Only Author and Title

Murai R, Okegawa Y, Sato N, Motohashi K (2021) Evaluation of CBSX proteins as regulators of the chloroplast thioredoxin system. Front Plant Sci. doi: 10.3389/fpls.2021.530376
Google Scholar: Author Only Title Only Author and Title

Nakano H, Yamamoto H, Shikanai T (2019) Contribution of NDH-dependent cyclic electron transport around photosystem I to the generation of proton motive force in the weak mutant allele of pgr5. Biochim Biophys Acta - Bioenerg 1860: 369–374
Google Scholar: Author Only Title Only Author and Title

Nielsen H, Engelbrecht J, Brunak S, Heijne G Von (1997) A neural network method for identification of Prokaryotic and Eukaryotic signal peptides and prediction of their cleavage sites. Int J Neural Syst 08: 581–599
Google Scholar: Author Only Title Only Author and Title

Nikkanen L, Toivola J, Trotta A, Diaz MG, Tikkanen M, Aro E-M, Rintamäki E (2018) Regulation of cyclic electron flow by chloroplast NADPH-dependent thioredoxin system. Plant Direct 2: e00093
Google Scholar: Author Only Title Only Author and Title

Ok SH, Yoo KS, Shin JS (2012) CBSXs are sensor relay proteins sensing adenosine-containing ligands in Arabidopsis. Plant Signal Behav 7: 664–7
Google Scholar: Author Only Title Only Author and Title

Okegawa Y, Motohashi K (2015) Chloroplastic thioredoxin m functions as a major regulator of Calvin cycle enzymes during photosynthesis in vivo. Plant J 84: 900–913
Google Scholar: Author Only Title Only Author and Title

Okegawa Y, Motohashi K (2020) M-type thioredoxins regulate the PGR5/PGRL1-dependent pathway by forming a disulfide-linked complex with PGRL1. Plant Cell tpc.00304.2020
Google Scholar: Author Only Title Only Author and Title

Pérez-Ruiz JM, Naranjo B, Ojeda V, Guinea M, Cejudo FJ (2017) NTRC-dependent redox balance of 2-Cys peroxiredoxins is needed for optimal function of the photosynthetic apparatus. Proc Natl Acad Sci U S A 114: 12069–12074
Google Scholar: Author Only Title Only Author and Title

Polge C, Thomas M (2007) SNF1/AMPK/SnRK1 kinases, global regulators at the heart of energy control? Trends Plant Sci. doi: 10.1016/j.tplants.2006.11.005
Google Scholar: Author Only Title Only Author and Title

Pulido P, Spínola MC, Kirchsteiger K, Guinea M, Pascual MB, Sahrawy M, Sandalio LM, Dietz KJ, González M, Cejudo FJ (2010) Functional analysis of the pathways for 2-Cys peroxiredoxin reduction in Arabidopsis thaliana chloroplasts. J Exp Bot 61: 4043–4054
Google Scholar: Author Only Title Only Author and Title

Ramon M, Ruelens P, Li Y, Sheen J, Geuten K, Rolland F (2013) The hybrid Four-CBS-Domain KINbγ subunit functions as the canonical γ subunit of the plant energy sensor SnRK1. Plant J 75: 11–25
Google Scholar: Author Only Title Only Author and Title

Rey P, Sanz-Barrio R, Innocenti G, Ksas B, Courteille A, Rumeau D, Issakidis-Bourguet E, Farran I (2013) Overexpression of plastidial thioredoxins f and m differentially alters photosynthetic activity and response to oxidative stress in tobacco plants. Front Plant Sci 4: 1–13
Google Scholar: Author Only Title Only Author and Title

Ruelland E, Lemaire-Chamley M, Le Maréchal P, Issakidis-Bourguet E, Djukic N, Miginiac-Maslow M (1997) An internal cysteine is involved in the thioredoxin-dependent activation of sorghum leaf NADP-malate dehydrogenase. J Biol Chem 272: 19851–19857

Google Scholar: Author Only Title Only Author and Title

Santarius KA, Heber U (1965) Changes in the intracellular levels of ATP, ADP, AMP and Piand regulatory function of the adenylate system in leaf cells during photosynthesis. BBA - Biophys Incl Photosynth 102: 39–54
Google Scholar: Author Only Title Only Author and Title

Scholl RL, May ST, Ware DH (2000) Seed and molecular resources for Arabidopsis. Plant Physiol 124: 1477–80
Google Scholar: Author Only Title Only Author and Title

Scott JW, Hawley S a., Green K a., Anis M, Stewart G, Scullion G a., Norman DG, Hardie DG (2004) CBS domains form energy-sensing modules whose binding of adenosine ligands is disrupted by disease mutations. J Clin Invest 113: 274–284
Google Scholar: Author Only Title Only Author and Title

Sekiguchi T, Yoshida K, Okegawa Y, Motohashi K, Wakabayashi K, Hisabori T (2020) Chloroplast ATP synthase is reduced by both f-type and m-type thioredoxins. Biochim Biophys Acta - Bioenerg 1861: 148261
Google Scholar: Author Only Title Only Author and Title

Shahbaaz M, Ahmad F, Imtaiyaz Hassan M (2015) Structure-based functional annotation of putative conserved proteins having lyase activity from Haemophilus influenzae. 3 Biotech 5: 317–336
Google Scholar: Author Only Title Only Author and Title

Shikanai T (2016) Chloroplast NDH: A different enzyme with a structure similar to that of respiratory NADH dehydrogenase. Biochim Biophys Acta - Bioenerg 1857: 1015–1022
Google Scholar: Author Only Title Only Author and Title

Shin JS, So WM, Kim SY, Noh M, Hyoung S, Yoo KS, Shin JS (2020) CBSX3-Trxo-2 regulates ROS generation of mitochondrial complex II (succinate dehydrogenase) in Arabidopsis. Plant Sci 294: 110458
Google Scholar: Author Only Title Only Author and Title

Stephan D, Slabber C, George G, Ninov V, Francis KP, Burger JT (2011) Visualization of plant viral suppressor silencing activity in intact leaf lamina by quantitative fluorescent imaging. Plant Methods. doi: 10.1186/1746-4811-7-25
Google Scholar: Author Only Title Only Author and Title

Stitt M, Lilley RM, Heldt HW (1982) Adenine nucleotide levels in the cytosol, chloroplasts, and mitochondria of wheat leaf protoplasts. Plant Physiol 70: 971–977
Google Scholar: Author Only Title Only Author and Title

Thormählen I, Meitzel T, Groysman J, Öchsner AB, von Roepenack-Lahaye E, Naranjo B, Cejudo FJ, Geigenberger P (2015) Thioredoxin f1 and NADPH-dependent thioredoxin reductase C have overlapping functions in regulating photosynthetic metabolism and plant growth in response to varying light conditions. Plant Physiol 169: pp.01122.2015
Google Scholar: Author Only Title Only Author and Title

Thormählen I, Zupok A, Rescher J, Leger J, Weissenberger S, Groysman J, Orwat A, Chatel-Innocenti G, Issakidis-Bourguet E, Armbruster U, et al (2017) Thioredoxins play a crucial role in dynamic acclimation of photosynthesis in fluctuating light. Mol Plant 10: 168–182
Google Scholar: Author Only Title Only Author and Title

Usuda H (1988) Adenine nucleotide levels, the redox state of the NADP system, and assimilatory force in nonaqueously purified mesophyll chloroplasts from maize leaves under different light intensities. Plant Physiol 88: 1461–1468
Google Scholar: Author Only Title Only Author and Title

Vaseghi M-J, Chibani K, Telman W, Liebthal MF, Gerken M, Schnitzer H, Mueller SM, Dietz K-J (2018) The chloroplast 2-cysteine peroxiredoxin functions as thioredoxin oxidase in redox regulation of chloroplast metabolism. Elife 7: 1–28
Google Scholar: Author Only Title Only Author and Title

Voon CP, Guan X, Sun Y, Sahu A, Chan MN, Gardeström P, Wagner S, Fuchs P, Nietzel T, Versaw WK, et al (2018) ATP compartmentation in plastids and cytosol of Arabidopsis thaliana revealed by fluorescent protein sensing. Proc Natl Acad Sci 201711497
Google Scholar: Author Only Title Only Author and Title

Waese J, Fan J, Pasha A, Yu H, Fucile G, Shi R, Cumming M, Kelley LA, Sternberg MJ, Krishnakumar V, et al (2017) ePlant: Visualizing and exploring multiple levels of data for hypothesis generation in plant biology. Plant Cell 29: 1806–1821
Google Scholar: Author Only Title Only Author and Title

Wang F, Yan J, Ahammed GJ, Wang X, Bu X, Xiang H, Li Y, Lu J, Liu Y, Qi H, et al (2020) PGR5/PGRL1 and NDH mediate far-red light-induced Photoprotection in response to chilling stress in Tomato. Front Plant Sci 11: 1–18
Google Scholar: Author Only Title Only Author and Title

Xiao B, Sanders MJ, Underwood E, Heath R, Mayer F V., Carmena D, Jing C, Walker PA, Eccleston JF, Haire LF, et al (2011) Structure of mammalian AMPK and its regulation by ADP. Nature 472: 230–233
Google Scholar: Author Only Title Only Author and Title

Yamori W, Sakata N, Suzuki Y, Shikanai T, Makino A (2011) Cyclic electron flow around photosystem I via chloroplast NAD(P)H dehydrogenase (NDH) complex performs a significant physiological role during photosynthesis and plant growth at low temperature in rice. Plant J 68: 966–976
Google Scholar: Author Only Title Only Author and Title

Yamori W, Shikanai T (2016) Physiological functions of cyclic electron transport around Photosystem I in sustaining photosynthesis and plant growth. Annu Rev Plant Biol 67: 81–106
Google Scholar: Author Only Title Only Author and Title

Yamori W, Shikanai T, Makino A (2015) Photosystem I cyclic electron flow via chloroplast NADH dehydrogenase-like complex performs a physiological role for photosynthesis at low light. Sci Rep 5: 13908
Google Scholar: Author Only Title Only Author and Title

Yoo KS, Ok SH, Jeong B-C, Jung KW, Cui MH, Hyoung S, Lee M-R, Song HK, Shin JS (2011) Single cystathionine b-synthase domain-containing proteins modulate development by regulating the thioredoxin system in Arabidopsis. Plant Cell 23: 3577–3594
Google Scholar: Author Only Title Only Author and Title

Yoshida K, Hara S, Hisabori T (2015) Thioredoxin selectivity for thiol-based redox regulation of target Proteins in Chloroplasts. J Biol Chem 290: 14278–14288
Google Scholar: Author Only Title Only Author and Title

Yoshida K, Hisabori T (2018) Determining the rate-limiting step for light-responsive redox regulation in chloroplasts. Antioxidants 7: 153
Google Scholar: Author Only Title Only Author and Title